UNIVERSITAT POLITÈCNICA DE CATALUNYA
BARCELONATECH
Escola Superior d'Enginyeries Industrial,
Aeroespacial i Audiovisual de Terrassa

Aeroelastic Study of the Flutter Conditions of an Aircraft Wing

BACHELOR FINAL THESIS

Document:

Report

Author/Authoress:

Guillermo Adroher Bolla

Director/Directress - Codirector/Codirectress:

Dr. David Roca Cazorla - Dr. Juan Carlos Cante Teran

Degree:

Bachelor's Degree in Aerospace Technologies Engineering

Examination Session:

Spring, 2022

Abstract

Aircraft wings are the responsible for planes to fly, they are the main structures providing lift so that the gravity is overcome. Therefore, one must ensure that instabilities do not appear because they can lead to fatal outcomes. Flutter is the most common instability that aircraft face, being of utmost importance to delay or eliminate its appearance. This work aims to create a MATLAB computational aeroelastic code that allows to couple the finite element structural development to an aerodynamic vortex method so to run a dynamic modal analysis which computes the flutter velocity of a parametrized wing. First, the wing geometry and parameters that affect its performance are defined, being the taper ratio, the sweep angle, the span, root and tip chord dimensions and a point mass simulating, for example, the engine. Then, the structural and aerodynamic coupling formulation and computational development are presented and, finally, the results of the parametric study are analyzed. Flutter can occur basically for bending and twisting motions and the results show clearly how important it is to distribute the inertia of a wing when computing the flutter speed, apart from making it have the most stiffness possible without adding much weight to the structure.

Resumen

Las alas de los aviones son las responsables de que éstos vuelen, son las estructuras que proporcionan principalmente la sustentación para vencer el efecto de la gravedad. Por lo tanto, hay que asegurarse de que no aparezcan inestabilidades que pueden llevar a resultados fatales. El *flutter* o aleteo es la inestabilidad más común a la que se enfrentan los aviones, siendo de suma importancia retrasar o eliminar su aparición. Este trabajo pretende crear un código aeroelástico computacional en MATLAB que permita acoplar el desarrollo estructural por elementos finitos a un método de vórtices aerodinámicos para realizar un análisis modal dinámico que calcule la velocidad de flutter de un ala parametrizada. En primer lugar, se define la geometría del ala y los parámetros que afectan a su rendimiento, siendo el ratio de cuerda de punta de ala entre cuerda raíz, el ángulo de flecha, las dimensiones de la envergadura y de las cuerdas y una masa puntual que simula, por ejemplo, el motor. A continuación, se presenta la formulación de acoplamiento estructural y aerodinámico y el desarrollo computacional y, finalmente, se analizan los resultados del estudio paramétrico. El flutter puede producirse básicamente por movimientos de flexión y torsión y los resultados muestran claramente la importancia de distribuir la inercia de un ala a la hora de calcular la velocidad de flutter, además de hacer que tenga la mayor rigidez posible sin añadir mucho peso a la estructura.

Contents

List of Figures

List of Tables

List of Abbreviations

- AoA: Angle of Attack
- AR: Aspect Ratio
- DOF: Degree Of Freedom
- EZASE: Easy Aeroservoelasticity
- FEM: Finite Element Method
- HVM: Horseshoe Vortex Method
- KJ: Kutta-Joukowsky
- LE: Leading Edge
- NACA: National Advisory Committee for Aeronautics
- SW: Sweep Angle
- TE: Trailing Edge
- TR: Taper Ratio
- VLM: Vortex Lattice Method

Chapter 1

Introduction

This first chapter summarizes the organization of the project by means of the aim, which describes the result sought, the scope, which expose the work packages and limits so to reach the result, the requirements, which are meant to be met in order to reach a correct solution and the justification, which details why the project is carried out.

1.1 Aim

The aim of this project is to build a computational program that models a wing structure subjected to aerodynamic loads in order to study its dynamic response, focusing on design parameters that trigger instabilities such as fluttering. The mathematical basis of the model is the Finite Element Method (FEM) and the software used, MATLAB. This work is addressed to students, professors or researchers who want to understand how structural and aerodynamic models of a structure are implemented, along with the coupling system that leads to obtaining the dynamic response.

1.2 Scope

The project will include:

- Study of the basis of the Finite Element Method (FEM), its implementation using MATLAB.
- Study of the structural implementation of beam and shell elements using the Gauss quadrature as an integral solver. Individual examples will be carried out before writing the final code summing all the contributions to the generated mesh.
- Study of the steady aerodynamic implementation of a wing structure, considering different panel methods such as the Horseshoe Vortex Method (HVM) or the Vortex Lattice Method (VLM).
- Study of the coupling system between the aerodynamic loads and the structural model.
- Study of the unstable phenomenon of flutter, its origins, consequences and possible solutions extracting data from the code. The design parameters of the external flow will be evaluated, focusing on their effect on the structure and on the flutter instability.
- Validation of the structural, aerodynamic and coupled codes using external sources which could be articles, university assignments or published projects.

The project will not include:

- Unsteady aerodynamic analysis, it would be needed in more advanced phases as future work.
- Addition of control surfaces so as to try to minimize the flutter effect and evaluate its response.
- Videos showing the wing's response or unstable behavior.

1.3 Requirements

The necessary requirements the project must meet are:

- Knowledge regarding computational methods such as the FEM and steady aerodynamics is needed.
- There must be a structural module which creates the mesh and builds the stiffness and mass matrices of it.
- There must be an aerodynamic module which computes the external loads of air into the wing.
- There must be a coupling module which adapts the aerodynamic external loads to external structural forces.
- There must be a post-process module which studies the dynamic response of the mesh and analyzes the flutter instability.
- The structural and aerodynamic models must be validated separately with external sources before writing the coupled code.
- The code implementation must be done using MATLAB.
- Conclusions and interpretations of the results must be synthesized at the end of the document.

1.4 Justification

Due to the elevated cost regarding prototype testing in the aerospace industry, nowadays computer programs are the ones responsible for carrying out those tests needed in initial design phases [1]. The state-of-the-art technology has reached amazing levels and universities start to teach students how to develop advanced codes which could help study a lot of phenomena in the future.

This project would help students, professors or researchers to understand and validate the most important instability phenomenon in an aircraft wing, fluttering. Apart from that, this code may be a preliminary study of real life problems and anyone who knows the basics of the FEM, computational structural and aerodynamic implementation of a structure would benefit from it, being able to modify and extend the program so to running more detailed analysis.

Chapter 2

Project Background & State of the Art

The project background and state of the art chapter seeks to put in context the phenomena of structural instabilities that take place in a plane wing. A historical evolution, since the first discoveries to nowadays research is exposed, along with the most relevant characters who made such discoveries. The description of these phenomena is focused on flutter instability, ending with a state of the art analysis with current developments in this field.

2.1 Historical Background

2.1.1 Aeroelastic instability in airplanes

Aeroelasticity is the study of the interaction between three concepts of forces; the aerodynamic, the inertia and the elastic forces [2]. Depending on the approach to the problem, there are two different cases:

- Static Aeroelasticity: It studies the variation in the aerodynamic forces' distribution of a fixed wing due to its elastic deformation. The ultimate effect is an unstable behavior, reducing the effectiveness of the control surfaces.
- Dynamic Aeroelasticity: It adds the phenomenon of flutter, which extracts energy from the air and induces vibrations on the fixed wing. A stall behavior and even the wing break can be faced.

Figure **1** shows the fields' interaction inside the aeroelasticty phenomena. Note that it is very complex to study, requiring of static and dynamic structural and aerodynamic knowledge.

On the other hand, a very important matter when talking about aeroelasticity is the fact that the wing deformation depends on loads while, at the same time, the loads' distribution depends on the deformation. One finds a coupled problem with a strong link between the two.

Inside the field of aeroeslasticity flutter is probably the most important phenomenon that aircraft face. As mentioned previously, it appears when the inertial forces are important (aerodynamic effect gains over structural resistance), thus dynamic instability appears. Catastrophic effects can be derived from flutter,

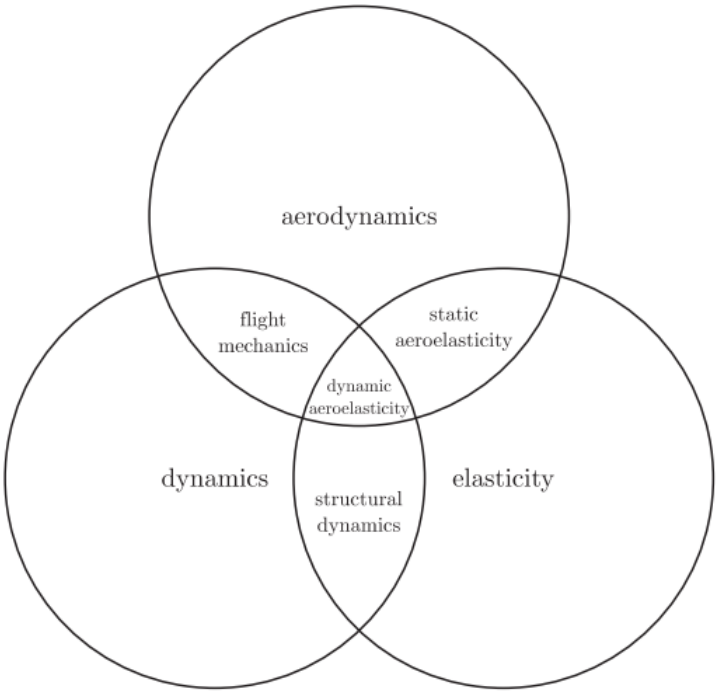

Figure 1 Schematic of the aeroelasticity field. (Source: [3])

leading to destruction of the wing, for example. That is why, when designing a lifting surface, it is vital to reduce unstable effects which could lead to failure, it is one of the major concerns for aircraft designers.

2.1.2 Aeroelasticity over the years

It goes without saying that aeroelastic phenomena have played a very important role throughout the history of aircraft flight. All the previous attempts of flying before the Wright brothers at the end of 1903 resulted in catastrophic failures due to the wing excess of flexibility and overloading [3].

However, it was not until some years before World War II that aerolelastic effects such as flutter began to be a concern. Combat planes started to fly at higher speed and control surfaces became key designs issues. Until then, the flutter solution was based on flying experience, being extremely unpredictable.

The first formal flutter test was carried out in 1935 in Germany in 1935, by Von Schlippe [4]. His idea was to make an aircraft vibrate at resonant frequencies, modifying the velocity and plotting the amplitude of the response. The points which had greater amplitude were the most probable conditions to develop an instability. An estimate of the results he obtained is shown inf Figure **2**.

At the same time, Theodore Theodorsen developed a mathematical theory to find flying instabilities. He was working at the National Advisory Committee for Aeronautics (NACA[1]) facility in the United States and published an article named *General theory of aerodynamic instability and the mechanism of flutter*. The basic hypotheses were to consider a flat plate and study its vibration response when withstanding an equivalent to flight speed conditions. The model was based on potential flow.

[1]The NACA, created in 1915, is one of the predecessors of the NASA (National Aeronautics and Space Administration), created in 1958.

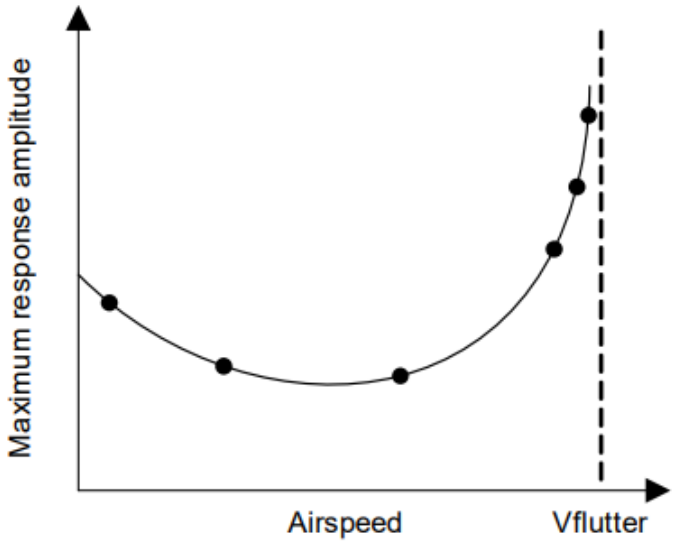

Figure 2 Von Schlippe flutter test results. (Source: [4])

Although the theory fundamentals were beginning to appear, there was not enough knowledge to find out closed solutions to the problems and establish security standards in the design of airplanes. Moreover, a lot of simplifying hypotheses made the model not applicable to real life, so the experimental approach was more accurate at that moment.

Beginning the 1950s the technology continued developing and experiments were carried out using new machines such as shakers, which could expand the test conditions. This new era permitted to do frequency sweeps and process data in a ground station. Planes started to carry excitation systems and real time experiments provided with accurate data to study the flutter case.

From the 1950s to the 1970s there were no deep changes in the experimental techniques but, in the mid 1970s, there was enough computational power to predict aeroelastic instabilities and solve advanced mathematical models. For example, the Fast Fourier Transform (FFT) allowed computing faster the flutter speed.

Nowadays, the approach continues to improve. Computers are very powerful and parameters such as damping can be estimated with several techniques.

2.2 State of the Art

As the nature of this project is to create a code so that the flutter instability can be studied in a planar wing, the most expanded computational methods and techniques to solve this instability are presented. In Chapter 5 the method used is discussed, assessing the computational cost versus the difficulty of implementation and precision of the solution.

These schemes aim to extract the roots which determine the flutter boundary, thus a margin of stability is established for flight conditions. Furthermore, they look to understand the physical mechanism that causes the instability.

Unsteady aerodynamics are studied, making it possible to bring the solution closer to real flight conditions. This type of aerodynamics assumes simple harmonic motion.

The explained methods used are summarized in the following list [3]:

- P-Method: It appeared as the classical stability solution to flutter instability, so it is the simpler method to understand. Its name comes from the dimensionless complex eigenvalue used to reach a solution, also named as reduced eigenvalue p. Unsteady aerodynamic models compute the loads induced by transient motion of the lifting surface and the result is obtained by solving a complex eigenvalue problem of the governing equations. It is computationally expensive, so nowadays big structures are not solved using this method.

- K-Method: It is also known as the V-g method. The main issue of this method is considering structural damping with their corresponding dissipating energy terms. The equations of motion for harmonic response are deduced making some hypotheses such as the forcing frequency and airspeed are known parameters.

  Then, the reduced frequency k is determined from the natural frequency w and the airspeed V. The equations are correct at all values of w and V, they are only true at the flutter point and they are treated as an eigenvalue problem. The results are presented in plots of frequency versus airspeed, supported by damping plots, which provide with a physical understanding of the phenomenon.

- PK-Method: This third scheme appeared because the K-Method is not formulated properly in terms of pure mathematics. Although the latter is quick, imposing that structural damping to a simple harmonic motion created controversy inside the industry. The PK-Method basically attempts to improve the K-Method allowing the reduced frequency to be complex. So, whether the root is or is not complex, the real part of it indicates the stable or unstable behavior of the system.

The aerospace industry nowadays uses the K-Method the most because it is the quickest one and provides a first approximation of the physical problem solution. However, when one wants to ensure the accuracy of the results the PK-Method is the chosen one.

Chapter 3

Theoretical Approach

This next chapter defines the basics of the type of mesh subject to study, along with the aerodynamic and structural coupling models that will lead to the study of the flutter instability. It aims to create a general picture of the problem and of the specific paths that lead to the solution. For further explanation of the structural and aerodynamic mathematical formulations see Appendices A and B.

It is structured in two modules: the wing geometry, including the elements, parameters, material properties and mass, and the coupling developments, both the static and dynamic.

3.1 Wing Geometry

When studying any structure the first step is always to define the geometry of it. Without a body it is impossible to create a mesh and perform a structural or aerodynamic analysis. In this section the simplified body geometry is defined, including all the basic parts which make up the structure. As the work focuses on analyzing the flutter phenomenon, the body to define is a wing. It is not necessary to define a full wing when carrying out analyses so, from this point on, the word wing makes reference to half of it.

3.1.1 Structural elements

The wing in this work is represented in Figure **3**. Its main element is a rectangular plate simulating the skin. However, other elements are added to strengthen the core structure such as spars and ribs. These additional elements are treated as beams, so two structural elements are present in the body, the plate and the beam.

- **Wing Skin:** The wing skin occupies all the wing surface, so the dimensions are to be established. These are

$$\begin{aligned} b &= 3.3540\,m \\ c &= 0.8380\,m \end{aligned} \tag{3.1}$$

where b refers to the semi-span and c to the chord and its thickness is established as $h = 3.06\,mm$. They are picked from a code titled EZASE (Easy Servoaeroelasticity) [5], written by a NASA doctor,

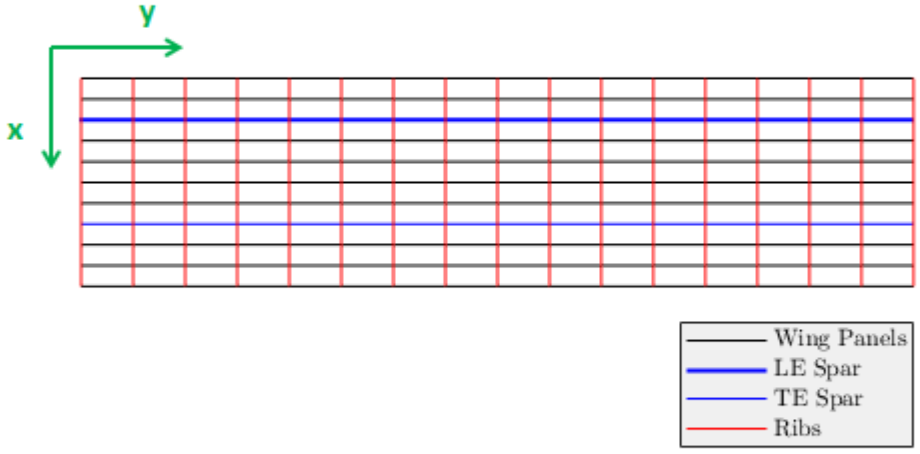

Figure 3 Original wing geometry with the global axes and the three structural parts; plates, spars and ribs.

so to make it easier to validate the structural and aerodynamic results obtained[1].

- **Spars:** The spars are the beam elements that cross all the wing's semi-span. They go from the root to the tip sections. In this case the wing contains two of them, one closer to the leading edge (LE) and the other one to the trailing edge (TE).

  Their cross-sections are not the same, it is necessary to add more weight close to the LE to ensure better stability and performance. Apart from that, to bring the study closer to a real wing, a linear taper is included. Close to the root chord the section is bigger and, moving away, getting closer to the tip, the section keeps reducing.

  Thus, the dimensions picked for both beams' cross-sections are

$$\begin{aligned} w_{i,LE} &= 25.40\,cm & w_{f,LE} &= 12.70\,cm \\ h_{i,LE} &= 50.80\,cm & h_{f,LE} &= 25.40\,cm \end{aligned} \tag{3.2}$$

$$\begin{aligned} w_{i,TE} &= 19.05\,cm & w_{f,TE} &= 12.70\,cm \\ h_{i,TE} &= 38.10\,cm & h_{f,TE} &= 25.40\,cm \end{aligned} \tag{3.3}$$

  where w and h refer to *width* and *height* and the subscripts i and f stand for *initial* and *final*, meaning closer to the root chord or to the tip, respectively.

- **Ribs:** The ribs cross the wing from the LE to the TE, they are placed along the chord direction and are also treated as beams. All of them have the same cross-section dimensions and linear taper, introduced to reduce the weight when moving away from the TE.

[1]This EZASE code includes two tutorials that allow validating FEM structural and VLM aerodynamic results.

The dimensions decided for the ribs are

$$\begin{aligned} w_{i,r} &= 25.40\,cm \qquad & w_{f,r} &= 12.70\,cm \\ h_{i,r} &= 50.80\,cm \qquad & h_{f,r} &= 25.40\,cm \end{aligned} \tag{3.4}$$

where the subscripts i and f mean the same as for the spars and r refers to the word *ribs*.

3.1.2 Wing parameters

So far the wing has been treated as a rectangle with constant span and chord. Nevertheless, the vast majority of airplanes that operate nowadays include geometrical modifications to improve the performance of the vehicle and reduce structural damage due to the big amount of aerodynamic forces they withstand. Among these modifications, the ones with most influence tend to be the wing taper, sweep and aspect ratio:

- **Taper Ratio (TR):** It defines the ratio of the tip chord, c_t, to the root chord, c_r, (see Figure **4**). If it is equal to 1, the chord is constant along the span while if it is different the chord is linearly modified.

$$TR = \frac{c_t}{c_r} \tag{3.5}$$

  Taper ratio is normally used to reduce weight at the tip of the wing because it is the zone where stall begins. Moreover, while reducing the weight the lifting surface there is also being reduced thus the aerodynamic force is lower.

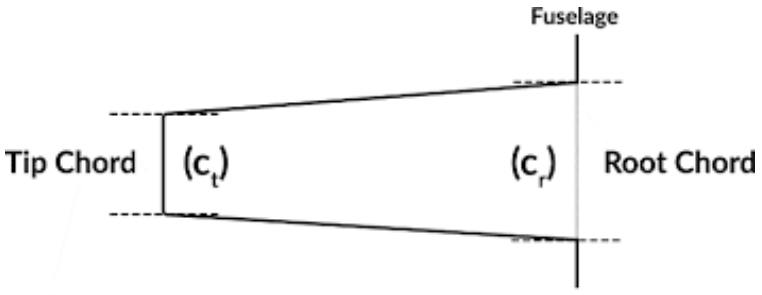

Figure 4 Wing root and tip chords, the two elements which define the taper ratio.

- **Sweep Angle (SW):** It is the angle between a line perpendicular to the fuselage's longitudinal axis and the line that goes from the quarter root chord to the quarter tip chord (see Figure **5**).

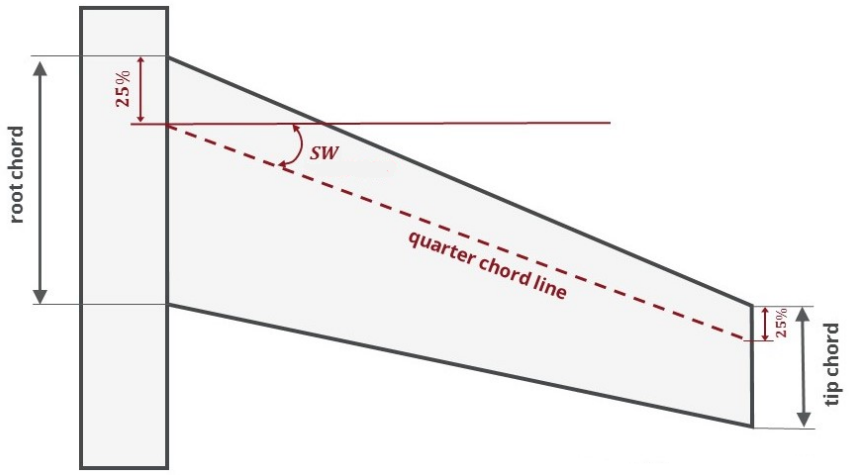

Figure 5 Representation of the sweep angle, together with the elements to define it.

The purpose of introducing wing sweep is to slow down the air when moving across the wing surface, it does not strike perpendicular to the fuselage's longitudinal axis.

- **Aspect Ratio (AR):** It defines the ratio of the wingspan to the wing mean chord. Mathematically it can be expressed as the square of the span divided by the wing surface.

$$AR = \frac{b^2}{S} = \frac{b^2}{b \cdot c} = \frac{b}{c} \tag{3.6}$$

However, in this project, the definition is a bit different. As the body corresponds to half of the wing, c refers to the mean chord, b to half of the span and S to half of the wing surface. So in this last equation the AR is really half of the value that one would obtain considering all the wing[2]. Analyzing the expression, as represented in Figure **6**, long span wings tend to have short chords thus they have high ARs while short span wings usually have longer chords, being the ARs considerably lower.

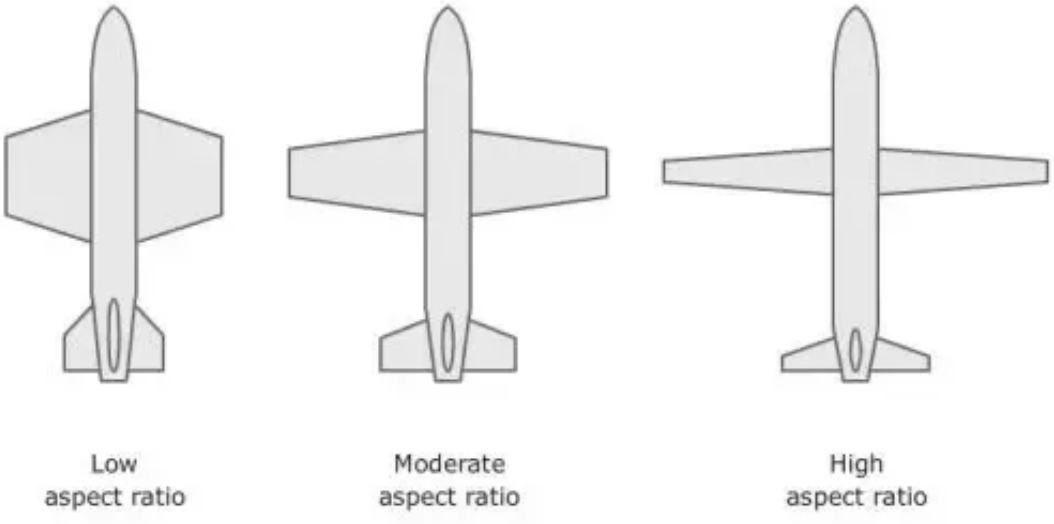

Figure 6 Examples of low, moderate and high aspect ratios in an airplane.

[2]If the Boeing B737-800 has an AR equal to 9.45, for example, the value of the ratio considering half of the wing would be 4.73 approximately.

Going back to the initial geometry depicted in Figure **3**, one can compute the three parameters just explained:

$$\begin{cases} TR = 1 \\ SW = 0^\circ \\ AR = 4 \end{cases}$$

Then, different wing geometries can be obtained by modifying the parameters both independently and together. Below are depicted three figures representing possible modifications of the original wing shape:

- The first one modifies the taper ratio only, the weep angle is kept at 0°.

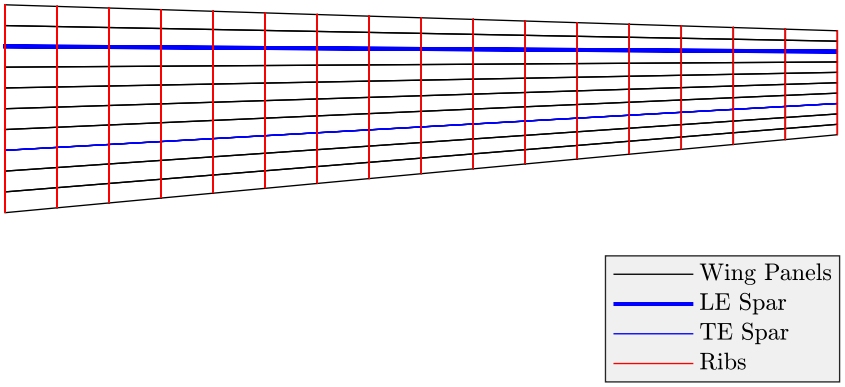

Figure 7 Wing geometry with $TR = 0.5$, $SW = 0^\circ$ and $AR = 5.33$.

- The second one keeps constant chord along the span, being the TR equal to 1, and introduces a positive sweep angle.

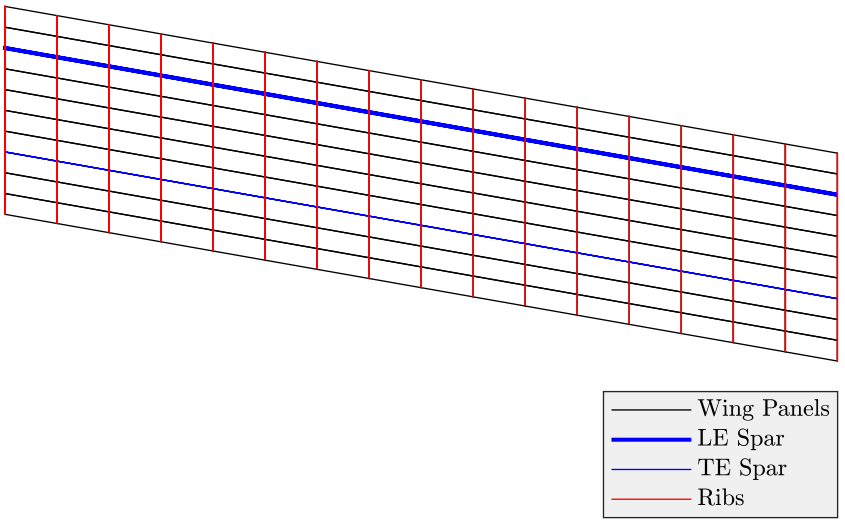

Figure 8 Wing geometry with $TR = 1$, $SW = 10^\circ$ and $AR = 4$.

- The last one modifies both the taper ratio and the sweep angle, so as to approach a real wing geometry.

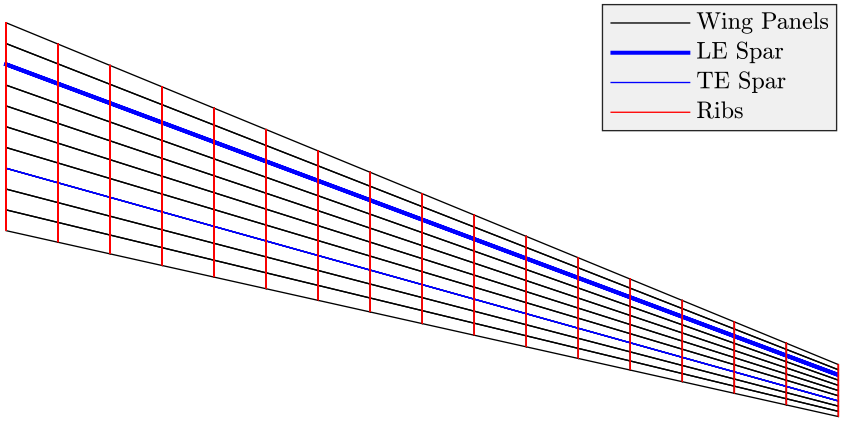

Figure 9 Wing geometry with $TR = 0.25$, $SW = 20°$ and $AR = 6.40$.

Notice that the sweep angle does not affect the aspect ratio, after all the wing surface is the same as if there was no angle and the chord does not take part in the formula.

3.1.3 Structural properties

Once the wing geometry is totally defined, from its original shape to possible modifications due to different parameters which can be introduced to change the planform, it is time to choose the material. In the aviation field weight is critical so the materials used must have low weight without losing resistance or rigidity, among others.

Therefore, the selected material for all the elements of the wing is Aluminum 6061-T6, T651. Its technical designation, weight composition and structural properties are described in the following tables.

Table 1 Material designation of the Aluminum 6061-T6, T651 alloy [6]

Material Designation		
Aluminum	**UNS[3] No.**	**ISO[4] No. R209**
6061	A96061	AlMg1SiCu

[3]The Unified Numbering System (UNS) is an alloy designation system which is widely used and accepted in the USA. It only defines the chemical composition, not the materials properties nor the testing methods, for example.
[4]The International Organization for Standardization has its standards to guarantee the quality of materials. Six different groups are defined to classify the metals.

Table 2 Weight composition of the Aluminum 6061-T6, T651 alloy [6]

Composition, wt%												
Si	**Fe**	**Cu**	**Mn**	**Mg**	**Cr**	**Ni**	**Zn**	**Ga**	**V**	**Ti**	**Other**	**Al, min**
0.4		0.15		0.8	0.04							
-	0.7	-	0.15	-	-	...	0.25	...	...	0.15	0.15	rem[5]
0.8		0.40		1.2	0.35							

Table 3 Structural properties of the Aluminum 6061-T6, T651 alloy [6]

Alloy & Temper	**Ultimate Tensile Strength UTS [MPa]**	**Tensile Yield Strength, TYS [MPa]**	**Ultimate Shearing Strength USS [MPa]**	**Fatigue Endurance Limit Se [MPa]**	**Modulus of Elasticity E [GPa]**
6061-T6, T651	310	275	205	95	68.9

A value which is not given in the tables but is very necessary to know is the density. As the weight quantity of *Al* goes from 95.85% to 97.21%, being the values very close to a 100%, the density is considered to be the same as for pure *Al*, $\rho_{Al} = 2700\,kg/m^3$.

Finally, estimating the Poisson's ratio from similar aluminum alloys the value of $\nu = 0.33$ is chosen. This way, the modulus of rigidity gives

$$G = \frac{E}{2\,(1+\nu)} = 26\,GPa \tag{3.7}$$

At this point, all the required data regarding the wing geometry, parametrization and materials is defined. The following chapters treat with the information presented in this one.

3.1.4 Wing's original shape mass

For the parametric study, it will be necessary to know the wing mass,M_{wing}, for the original planform. The easiest way is to divide the computation into the different parts.

- **Wing Skin:** The cross section is constant so the computation is simple:

$$M_{skin} = h\,c_r\,b\,\rho_{Al} = 23.2216\,kg \tag{3.8}$$

  The parameter h refers to the plate thickness, being 3.06 mm, while the other dimensions are already defined.

- **Spars:** Both the LE and TE spars are computed with integrals because they depend linearly on y.

[5]It means *remaining*, because the percentages are ranges and no fixed value can be given to the minimum %Aluminum.

Being the expressions that define the height, H, and width, W, of the rectangular spars' cross section

$$\begin{aligned} H(y) &= \frac{H_f - H_i}{b}\, y + H_i \\ W(y) &= \frac{W_f - W_i}{b}\, y + W_i \end{aligned} \tag{3.9}$$

the integral to compute the mass look like

$$M_{spar} = \int_0^b \rho_{Al}\, A(y)\, dy = \rho_{Al} \int_0^b H(y)\, W(y)\, dy = \frac{\rho_{Al}\, b}{3} \left(H_f W_f + H_i W_i + \frac{H_f W_i + H_i W_f}{2} \right) \tag{3.10}$$

and introducing the dimensions in Equations 3.2 and 3.3 one gets

$$\begin{aligned} M_{spar,LE} &= 6.8162\, kg \\ M_{spar,TE} &= 4.6253\, kg \end{aligned} \tag{3.11}$$

- **Ribs:** For the mass of the ribs, the cross sections vary also but, in this case, along x and the integral is the same changing the limits, now from 0 to c_r. There are 17 ribs in total and each of them is the same in dimensions so the integrals that define the cross section height and width are

$$\begin{aligned} H_r(x) &= \frac{H_{r,f} - H_{r,i}}{c_r}\, x + H_{r,i} \\ W_r(x) &= \frac{W_{r,f} - W_{r,i}}{c_r}\, x + W_{r,i} \end{aligned} \tag{3.12}$$

while the integral to compute the total mass of all the ribs states

$$\begin{aligned} M_{ribs} &= n_{ribs} \int_0^{c_r} \rho_{Al}\, A(x)\, dx = n_{ribs}\, \rho_{Al} \int_0^{c_r} H_r(x)\, W_r(x)\, dx \\ &= n_{ribs} \frac{\rho_{Al}\, c_r}{3} \left(H_{r,f} W_{r,f} + H_{r,i} W_{r,i} + \frac{H_{r,f} W_{r,i} + H_{r,i} W_{r,f}}{2} \right) \end{aligned} \tag{3.13}$$

Introducing the dimensions in Equation 3.4, the total mass of them gives

$$M_{ribs} = n_{ribs}\, 1.7030 = 28.9515\, kg \tag{3.14}$$

where $1.7030\, kg$ is the mass of a single rib element.

Finally, the total mass of the wing for the case of $TR = 1$, $SW = 0°$ and $AR = 4$ is

$$M_{wing}(TR = 1, SW = 0, AR = 4) = M_{skin} + M_{spar,LE} + M_{spar,TE} + M_{ribs} = 63.6146\, kg \tag{3.15}$$

Not to make the computation of the wing mass more difficult, when modifying any of the parameters exposed previously it will be computed using the surfaces' ratio, that is to say, calculating the surface of the wing planform when applying different parameters and dividing it by the original. Then, the mass will be multiplied by this ratio to obtain the new value.

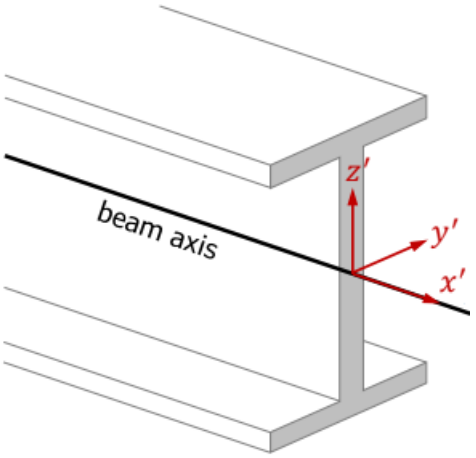

Figure 10 Beam local axes considering an arbitrary I cross-section. (Source: [7])

3.2 Structural Basics

In this section, two theories are exposed, the Timoshenko for beams and the Reissner-Mindlin for flat plates. The hypotheses considered are presented, for a detailed explanation see Appendix A.1. In the Appendix, both models are described from the hypotheses to the FEM application, going through the mathematical formulation.

3.2.1 Timoshenko beam theory

The Timoshenko beam theory comes from the Euler-Bernoulli model, erasing one hypothesis from the latter that make the results more accurate.

Hypotheses of Timoshenko

To begin with the Euler-Bernoulli basis is exposed. The beam local axes are depicted in Figure **10**.

- For shear loads applied on y' and bending moments about z' [7]:
  - Deflection $u_{y'}$ of the points on a cross- section are small and equal to the deflection of the beam axis.
  - Lateral displacement $u_{z'}$ is zero.
  - Cross-sections to the beam axis remain plane.
  - Cross-sections to the beam axis remain orthogonal to the beam axis after deformation.
- Equivalently, for shear loads applied on z' and bending moments about y' [7]:
  - Deflection $u_{z'}$ of the points on a cross- section are small and equal to the deflection of the beam axis.
  - Lateral displacement $u_{y'}$ is zero.

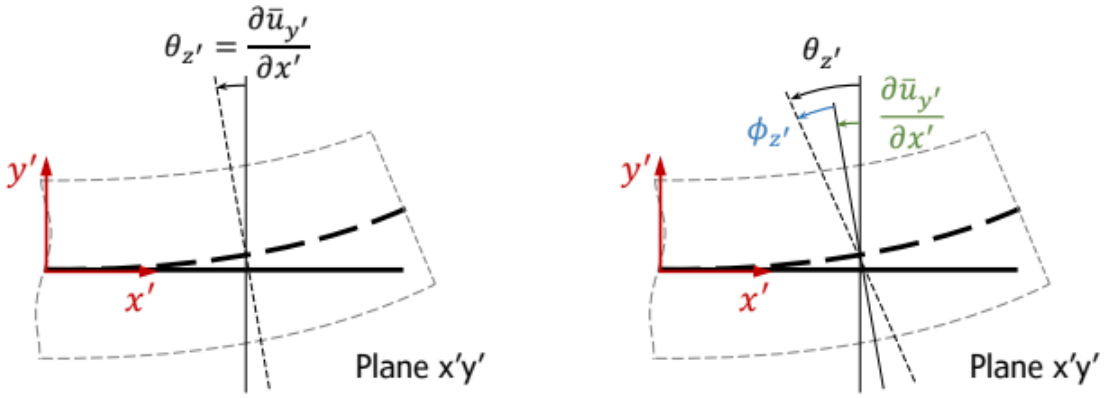

Figure 11 Plane $x'y'$ deflection comparison between the Euler-Bernoulli and the Timoshenko theories. (Source: [7])

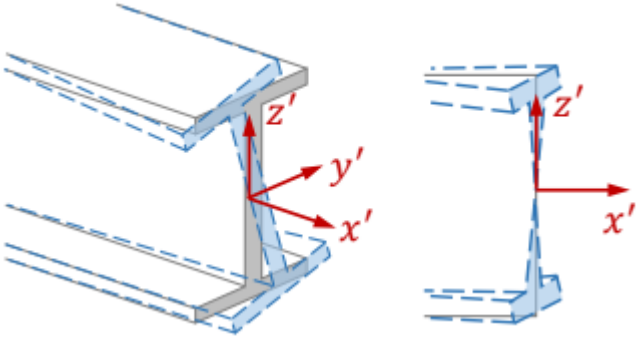

Figure 12 Rigid-body rotation deformation (left) and warping phenomenon (right). (Source: [7])

At this point, the only difference between the Timoshenko model and the Euler-Bernoulli is the removal of the last hypothesis when applying shear loads on y' and bending moments about z'. Timoshenko erases the restriction for the cross-sections to be orthogonal to the beam axis after deformation, obtaining a more realistic model.

Now, twist is the only type of deformation which is not considered yet. The Saint-Venant theory is accurate when considering twist, its hypotheses being the following.

- For beams with circular cross-section subjected to a twist moment about x' [7]:
  - The motion of each cross-section is a rigid body rotation about x'.
  - All points in the cross-section remain plane (there are no displacements in the x' direction).

When the cross-section of the beam is not circular, the last hypothesis is not true and displacements in the x' direction appear. This type of displacements are called *warping* (see Figure **12**).

When considering the warping phenomenon in practice, a twist constant is created so to compute the equivalent of the total deformation energy of the beam.

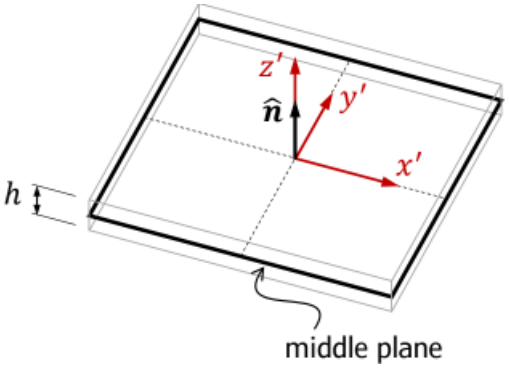

Figure 13 Thin-plate middle plane and its local axes. (Source: [8])

3.2.2 Reissner-Mindlin plate theory

Although the Reissner-Mindlin theory comes from the Kirchhoff thin plate theory, the results are more precise than the latter. There is a restriction of the model which is not considered.

Hypotheses of Reissner-Mindlin

Firstly, the Kirchhoff basis for thin plates is stated (based on [8]). The displacements are computed in the middle plane (see Figure **13**), due to the thin thickness assumption.

- Points along the normal to the middle plane have the same vertical displacement (the thickness remains constant during deformation).
- Normal stress component is negligible, $\sigma_z \approx 0$ (plane stress assumption).
- A straight line normal to the undeformed middle plane remains straight after deformation.
- Points on the middle plane only move vertically ($\bar{u}_{x'} = \bar{u}_{y'} = 0$).
- A straight line normal to the undeformed middle plane remains normal to the deformed middle plane.

At this point, the only difference between the Reissner-Mindlin model and the Kirchhoff is the removal of the last hypothesis. The Ressner-Mindlin formulation erases the restriction for a straight line normal to the undeformed middle plane to remain normal to the deformed middle plane, thus a more realistic approximation is considered.

3.3 Aerodynamic Basics

After presenting the bases of the structural model, this section aims to describe the basic formulation of the aerodynamic problem wanted to solve. The fundamentals of the theory exposed apply for inviscid and incompressible flow, simplifying the model without losing accuracy in the results. Further mathematical and computational explanation is presented in Appendix B.

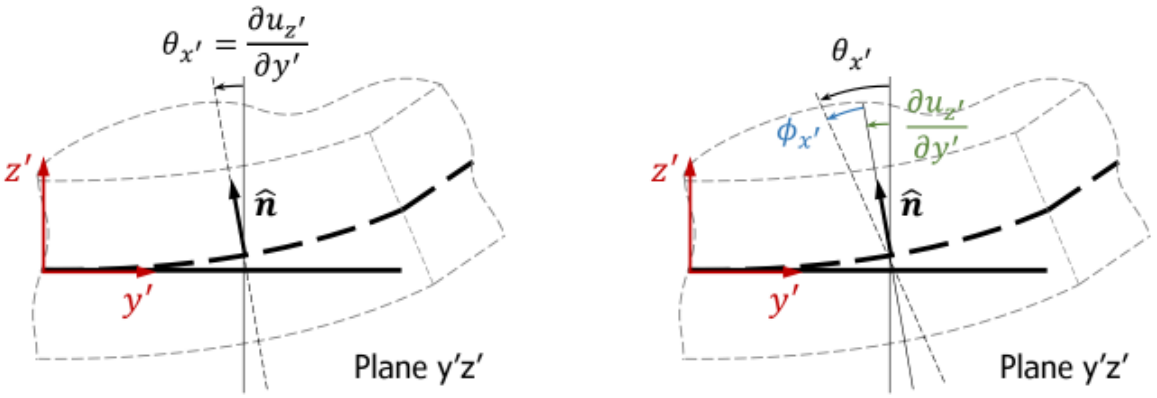

Figure 14 Plane $y'z'$ mid-plane deflection comparison between the Kirchhoff and the Reissner-Mindlin theories. (Source: [8])

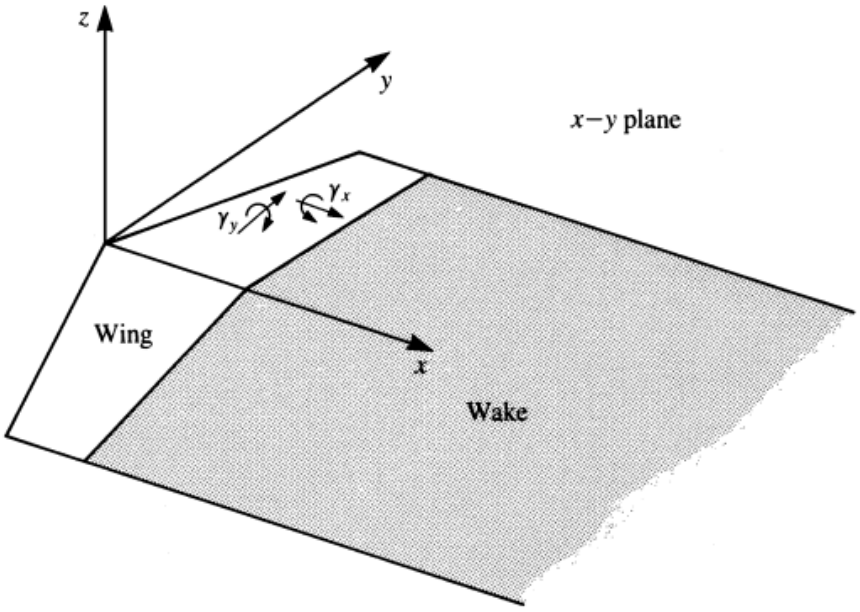

Figure 15 Lifting surface model of a 3D wing. (Source: [1])

3.3.1 Zero-Thickness Cambered Wing at AoA–Lifting Surfaces

Now that the basic aerodynamic concepts are already introduced, it is time to formulate the problem adapted to a finite wing. The element treated as a wing is called lifting surface and it is depicted in Figure **15**.

The problem to be solved is

$$\nabla^2 \Phi = 0 \tag{3.16}$$

with the boundary condition that requires no flow across the surface (in this cased evaluated at z = 0) shown in Figure **16**

$$\frac{\partial \Phi}{\partial z}(x, y, 0\pm) = Q_\infty \left(\frac{\partial \eta_c}{\partial x} - \alpha \right) \tag{3.17}$$

Because of the small-disturbance approximation the wake is also considered to be planar (placed on the z = 0 plane).

As the aerodynamic model is based on vortex distribution, this zero-thickness cambered wing at AoA lifting

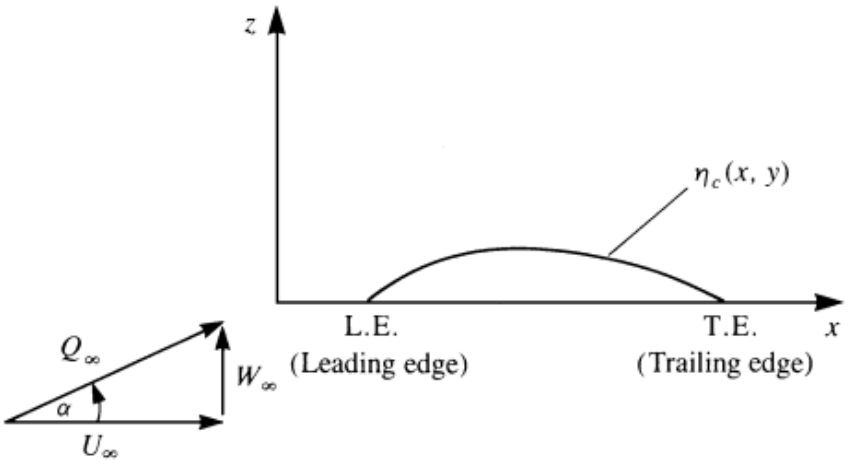

Figure 16 Nomenclature used for the definition of the lifting wing problem. (Source: [1])

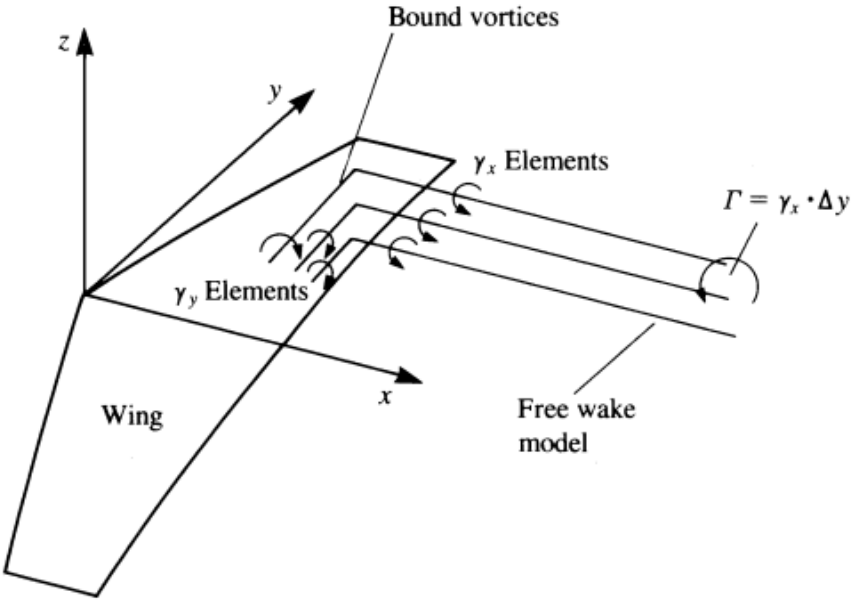

Figure 17 Vortex representation for the lifting surface model. (Source: [1])

surface problem considers only the vortex solution. Vortex line distributions are used over the wing and the wake. By considering the Biot-Savart law in differential form,

$$d\boldsymbol{V} = \frac{-1}{4\pi} \frac{d\Gamma \boldsymbol{r} \times d\boldsymbol{l}}{r^3} \tag{3.18}$$

where $d\boldsymbol{V}$ is the velocity due to a vortex line element $d\boldsymbol{l}$ with a strength of $d\Gamma$, one can get the component of velocity normal to the wing (downwash).

This downwash is induced by vortices distributed over the wing and wake as in Figure **17**, where the elements

that point in the y direction are denoted as γ_y[6] and the ones pointing in the x direction are denoted as γ_x.

$$u_z\left(x,y,z\right) = \frac{-1}{4\pi}\int_{\text{wing+wake}} \frac{\gamma_y(x-x_0)-\gamma_x(y-y_0)}{r^3}dx_0\,dy_0 \tag{3.19}$$

Notice that thee are two unknowns (γ_x and γ_y) and one equation. However, thanks to the first Helmholtz theorem in Appendix B.1.1 the strength of a vortex filament is constant along its length. This way, considering that the wing consist of numerous infinitesimal vortex lines then at any point

$$\left|\frac{\partial\gamma_x}{\partial x}\right| = \left|\frac{\partial\gamma_y}{\partial y}\right| \tag{3.20}$$

and the unknowns reduce to only one.

Finally, to construct the lifting surface equation for the unknown $\gamma = \gamma_x = \gamma_y$ the wing induced downwash (Equation 3.19) must be equal and opposite in sign to the normal component of the freestream velocity (Equation 3.17)

$$\frac{-1}{4\pi}\int_{\text{wing+wake}} \frac{\gamma_y(x-x_0)-\gamma_x(y-y_0)}{\left[(x-x_0)^2+(y-y_0)^2\right]^{3/2}}dx_0\,dy_0 = Q_\infty\left(\frac{\partial\eta_c}{\partial x}-\alpha\right) \tag{3.21}$$

This result allows to compute the velocity field distribution.

3.4 Aeroelastic Coupling

The main idea of the aerodynamic and structural coupling is to relate the two theories with the objective of running a modal analysis. This analysis is an eigenvalue problem that gives different dynamic pressures as eigenvalues and vectors of vertical component velocities as eigenvectors.

First of all, the static coupling is formulated and then, the case is extended to dynamic.

3.4.1 Static coupling

Static coupling, as the name itself indicates, considers the panels to remain still. This way, the angle of attack they have with respect to the freestream velocity does not change.

To begin with, a general matrix equation relating the stiffness matrix, displacements and an external force states

$$[K]\{u\} = \{f\} \tag{3.22}$$

where $\{u\}$ is the vector of displacements for the nodes of the body and $\{f\}$ is the external force vector, also distributed across all the nodes. This equation is the base of all the structural problems solved computationally.

So, the idea is to relate, on the one hand, the aerodynamic angles of attack to the displacements u and, on the other hand, the circulations to the external forces f.

[6]The variable γ is known as the circulation density and it is computed dividing the total circulation of an airfoil, for example, by its length.

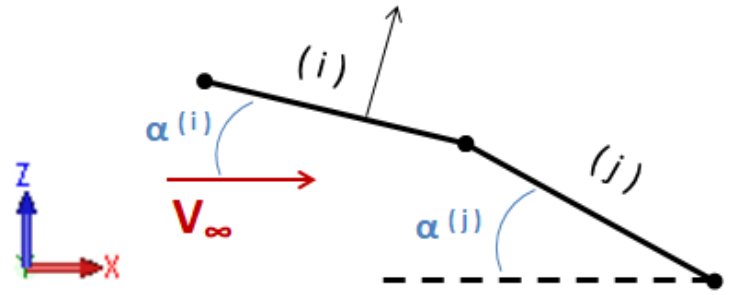

Figure 18 Panels' angle of attack (AoA) representation in the global coordinates' system.

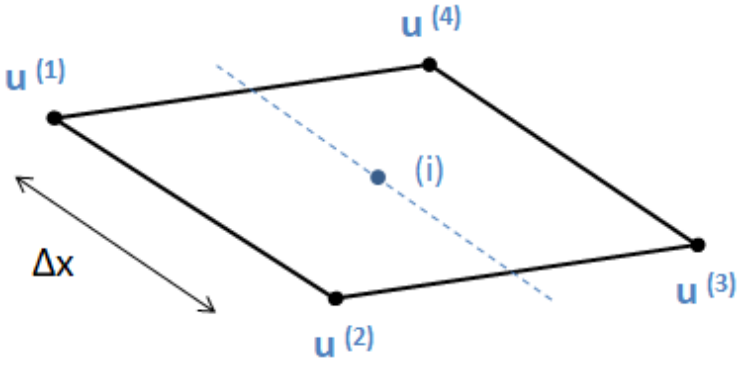

Figure 19 Panel nodes' displacements and dimensions along with its central point.

From the aerodynamic matrix system of equations one gets

$$[A]\{\Gamma\} = -V_\infty \{\alpha\} \tag{3.23}$$

where $[A]$ is the influence coefficients matrix, $\{\Gamma\}$ the circulations vector, V_∞ the freestream velocity and $\{\alpha\}$ the angles of attack vector. These angles of attack are depicted in Figure **18** along with the freestream velocity vector and the global coordinates' system.

Then, to find the matrix which relates the AoA with the displacements an operation like the following needs to be done:

$$\{\alpha\} = [D]\{u\} \tag{3.24}$$

where $[D]$ is the desired matrix, the one that relates the AoA and the vertical displacements.

If matrix $[D]$ is added to Equation 3.23 one gets

$$[A]\{\Gamma\} = -V_\infty [D]\{u\} \tag{3.25}$$

and isolating the circulation,

$$\{\Gamma\} = -V_\infty [A]^{-1} [D]\{u\} \tag{3.26}$$

Notice that it is inevitable not to have the inverted influence coefficients matrix, which is an expensive computational step. To find this matrix $[D]$ it is necessary to do the small angles' assumption. Taking a look

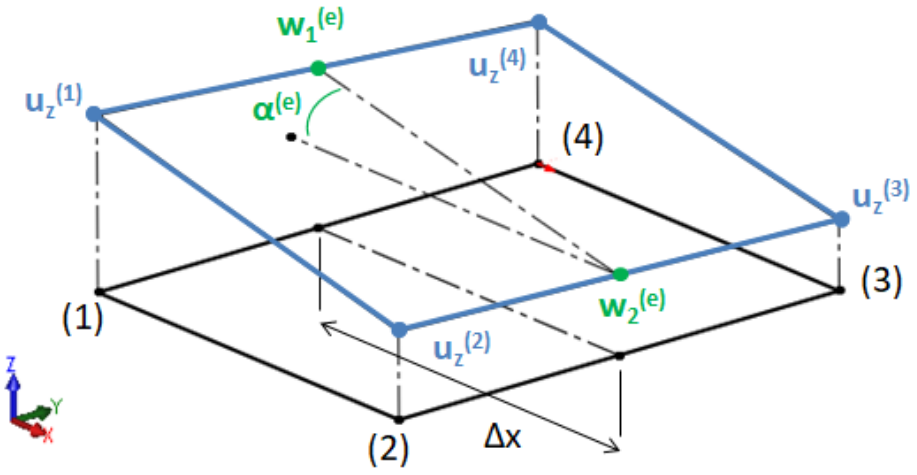

Figure 20 Panel initial and final positions with the nodes mean displacements in the y direction.

at the element in Figure **19**, the mean vertical displacement of the nodes in segments 1-4 and 2-3 can be computed as

$$\begin{aligned} w_{14} &= \frac{u_z^{(1)} + u_z^{(4)}}{2} \\ w_{23} &= \frac{u_z^{(2)} + u_z^{(3)}}{2} \end{aligned} \tag{3.27}$$

and, if the tangent is approximated to a function, the AoA looks like

$$\alpha \approx \frac{w_{14} - w_{23}}{\Delta x} \tag{3.28}$$

or introducing the vertical displacement of each node of the element,

$$\alpha \approx \frac{u_z^{(1)} + u_z^{(4)} - u_z^{(2)} - u_z^{(3)}}{2\,\Delta x} \tag{3.29}$$

Figure **20** depicts the initial and final element positions, making it easier to understand the process followed for each element.

In matrix form the last operation can be written as

$$\alpha^{(i)} = \frac{1}{2\,\Delta x^{(i)}} \begin{bmatrix} 1 & -1 & -1 & 1 \end{bmatrix} \begin{Bmatrix} u^{(1)} \\ u^{(2)} \\ u^{(3)} \\ u^{(4)} \end{Bmatrix} \tag{3.30}$$

where matrix $[D]$ is purely geometrical and appears when combining all the elemental matrices like that one in the corresponding positions.

Now that the AoA and displacements are related, it is time to work on the external force vector. Another matrix is to be found, one that satisfies the relationship:

$$\{f\} = [Q]\,\{\Gamma\} \tag{3.31}$$

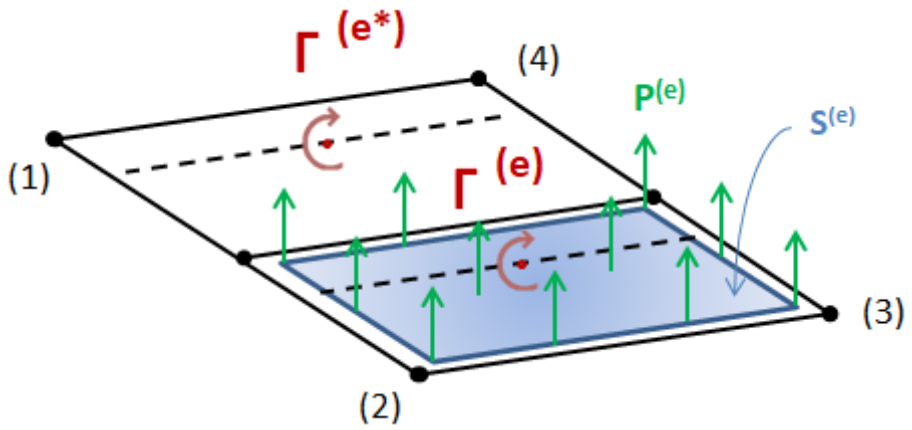

Figure 21 Representation of the external lift force acting on a panel (e) with the adjacent panel closer to the LE (e^*).

Substituting Equation 3.26 into this last one, it becomes

$$\{f\} = -V_\infty [Q] [A]^{-1} [D] \{u\} \tag{3.32}$$

where the $[Q]$ matrix is not only geometrical but also aerodynamic. So as to understand the mathematical operations Figure **21** shows a random element with the necessary parameters to compute the matrix. The external force in this case is the lift and it is natural to think that, in any element e, it can be divided by the number of nodes so each node's contribution is found. Using the Kutta-Joukoswky (KJ) theorem the lift can be computed with the expression

$$L^{(e)} = \rho_\infty V_\infty \left(\Gamma^{(e)} - \Gamma_0^{(e^*)}\right) \Delta y^{(e)} \tag{3.33}$$

where e refers to the element studied and e^* to the adjacent element closer to the LE (it is only needed for panels that are not in the LE).

Notice that the density and freestream velocity can go out because they are constants and the $[Q]$ matrix depends only on geometrical parameters. For a node in a LE panel, the contribution to the matrix is

$$Q^{(e)} = \frac{\Delta y^{(e)}}{4} \tag{3.34}$$

but for all the other nodes, the circulation of the adjacent node closer to the LE needs to be subtracted, becoming the contribution

$$\begin{aligned} Q^{(e)} &= \frac{\Delta y^{(e)}}{4} \\ Q^{(e^*)} &= \frac{\Delta y^{(e)}}{4} \end{aligned} \tag{3.35}$$

Once the matrix is found, extracting the mentioned constants makes Equation 3.32 become

$$\{f\} = -\rho_\infty V_\infty^2 [Q] [A]^{-1} [D] \{u\} \tag{3.36}$$

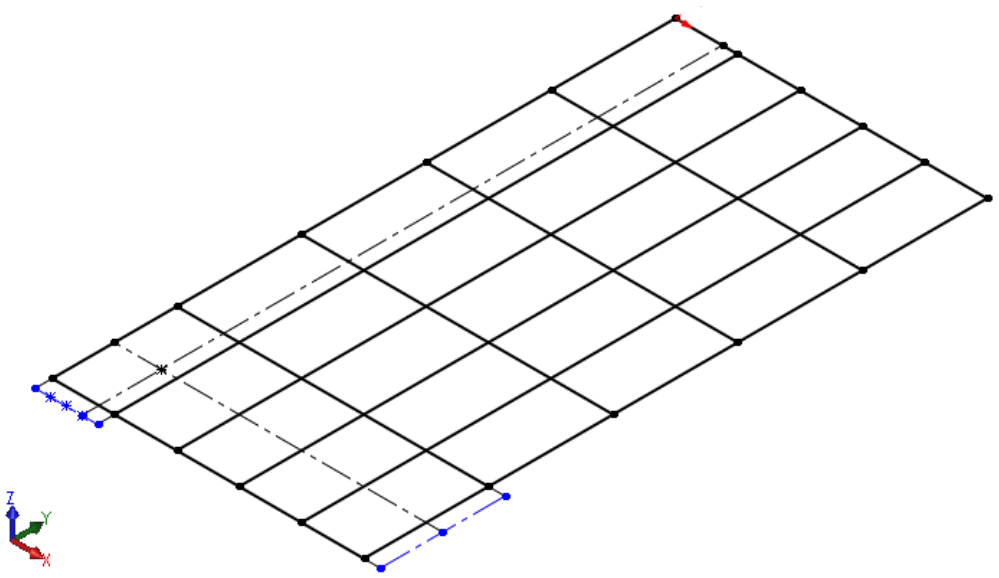

Figure 22 Wing discretization with the position of the first collocation point.

and if a unitary fraction is introduced, the dynamic pressure appears,

$$\{f\} = -\frac{2}{2}\rho_\infty V_\infty^2 \left[Q\right]\left[A\right]^{-1}\left[D\right]\{u\} = -\frac{1}{2}\rho_\infty V_\infty^2 \cdot 2\left[Q\right]\left[A\right]^{-1}\left[D\right]\{u\} = -q_\infty \cdot 2\left[Q\right]\left[A\right]^{-1}\left[D\right]\{u\} \tag{3.37}$$

Finally, introducing Equation 3.36 into 3.22 the equation which defines structural and aerodynamic static coupling appears:

$$\left[K\right]\{u\} = -q_\infty \cdot 2\left[Q\right]\left[A\right]^{-1}\left[D\right]\{u\} \tag{3.38}$$

Taking the common factor of the vector of displacements it can be equalled to zero as

$$\left(\left[K\right] + q_\infty \cdot 2\left[Q\right]\left[A\right]^{-1}\left[D\right]\right)\{u\} = \{0\} \tag{3.39}$$

Equation 3.39 has the form of a typical eigenvalue problem in structural dynamics, formulated as

$$\left(\left[K\right] - \lambda_i\left[M\right]\right)\{\phi_i\} = 0 \tag{3.40}$$

where $[K]$ refers to the stiffness matrix, λ_i to the eigenvalue of ode i, $[M]$ to the mass matrix and $\{\phi_i\}$ to the eigenvector of mode i.

In this case, matrix $[K]$ remains the same, as it is the main indicator of the structural properties of the body. However, what changes is matrix $[M]$. Now an aerodynamic matrix has been found, so matrix $[M]$ becomes a combination which includes the influence coefficients matrix, the heart of the aerodynamic formulation. Figure **22** shows the wing panels and the position of the collocation point.

Taking a look at Equation 3.40, the dynamic pressure with opposite sign is the eigenvalue and the vector of displacements the eigenvector.

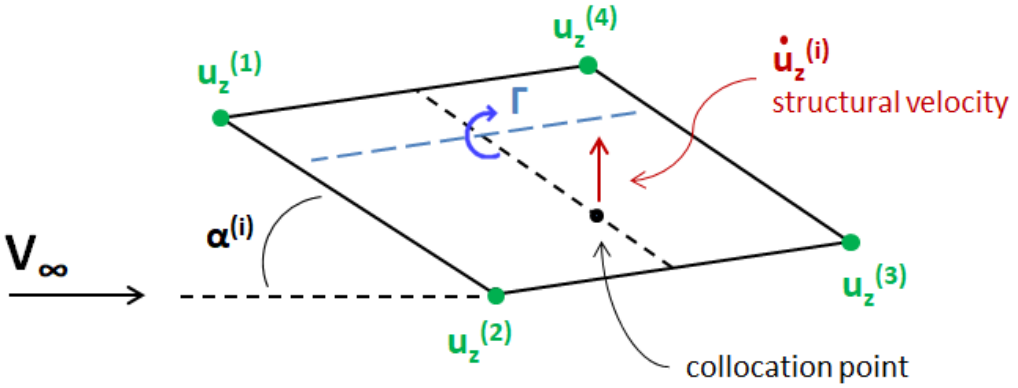

Figure 23 Representation of an element for the case of dynamic coupling with all the main parameters involved in the mathematical formulation.

When solving it computationally it is better to compute the analog to the mass matrix, in this case the aerodynamic $\left(2\,[Q]\,[A]^{-1}\,[D]\right)$, with negative sign so the eigenvalue q_∞ gives directly the result with the correct sign. This way, the step to change the eigenvalue sign is avoided.

3.4.2 Dynamic coupling

Dynamic coupling is an extension of the static case. As the name indicates the panel is not still anymore so an additional term needs to be added. Considering a panel i as the one in Figure **23**, there are three terms that contribute to the vertical velocity of the panel:

$$V_\infty\,\alpha^{(i)} - \dot{u}_z^{(i)} + \sum_j v_i(\Gamma_j) \tag{3.41}$$

The first and the last contributions also appeared in the static case but the middle one is new. It refers to the velocity of the panel.

As the last term includes the induced velocities in panel i by the other panels j, it can be represented with the influence coefficients matrix multiplied by the circulations vector. Thanks to that, the last equation transforms into

$$[A]\,\{\Gamma\} = -V_\infty\,\alpha^{(i)} + \dot{u}_z^{(i)} \tag{3.42}$$

If the circulations vector is isolated, it becomes

$$\{\Gamma\} = -V_\infty\,[A]^{-1}\,\alpha^{(i)} + [A]^{-1}\,\dot{u}_z^{(i)} \tag{3.43}$$

where the first term is identical to the one obtained in the static case and the second one is new. Therefore, matrices $[D]$ and $[Q]$ computed in the previous subsection remain the same and apply for the transformation of the first term changing the dependency of the AoA by the displacements vector.

Then, for the second term one last matrix needs to be found, relating the vertical displacements vector (in

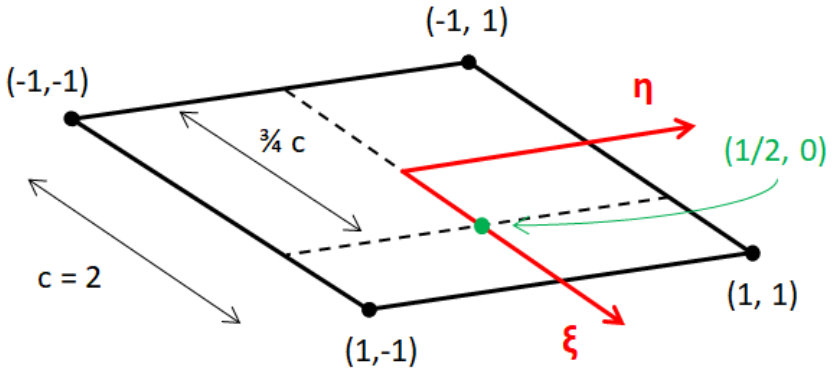

Figure 24 Isoparametric coordinates of the collocation point in an element.

the z direction) to the degrees of freedom (DOFs) displacements:

$$\{\dot{u}_z\} = [E]\,\{\dot{u}\} \tag{3.44}$$

Introducing that inside Equation 3.43, it becomes

$$\{\Gamma\} = -V_\infty\,[A]^{-1}\,[D]\,\{u\} + [A]^{-1}\,[E]\,\{\dot{u}\} \tag{3.45}$$

The process to compute $[E]$ is very simple, the matrix is filled with zeros in all the positions except for the DOF representing the z displacement at each node, which will be filled with the value of the shape function corresponding to that node.

As seen in Figure **23**, the structural velocity is interpolated at the collocation point and the shape function is computed using isoparametric coordinates. The collocation point of a random element using these coordinates is depicted in Figure **24**. The shape function of a quadrilateral element e is, at a point (ξ_c, η_c), characterized by the equation in Annex A.2.3)

$$N^{(e,i)}(\xi_c, \eta_c) = \frac{1}{4}\,(1 + a_i\,\xi_c)\,(1 + b_i\,\eta_c) \tag{3.46}$$

where a_i and b_i are two vectors containing the coordinates of the four nodes that make up the element. Following the anticlockwise direction the values can also be found in Annex 2.1.3.

At this point, it is necessary to build the dynamic matrix system of equations. The general expression for structural vibration problems is

$$[M]\,\{\ddot{u}\} + [C]\,\{\dot{u}\} + [K]\,\{u\} = \{f\} \tag{3.47}$$

where $[M]$ is the mass matrix, $[C]$ the damping matrix, $[K]$ the structural matrix and $\{f\}$ the external force vector.

Both the mass and structural matrices are directly found with the FEM formulation (see Appendix A.2) but

the damping matrix and the external force vector depend strictly on aerodynamic parameters.

Considering the circulation vector in Equation 3.45 and introducing it in the external force vector of the static case (Equation 3.31) one gets

$$\{f\} = \rho_\infty V_\infty [Q] \left(-V_\infty [A]^{-1} [D] \{u\} + [A]^{-1} [E] \{\dot{u}\}\right) \tag{3.48}$$

and extending the parenthesis together with making the dynamic pressure q_∞ appear, it transforms into

$$\{f\} = -q_\infty \cdot 2 [Q] [A]^{-1} [D] \{u\} + \frac{q_\infty}{V_\infty} \cdot 2 [Q] [A]^{-1} [E] \{\dot{u}\} \tag{3.49}$$

Reorganizing and making it look like the general expression for structural vibration problems presented before, one obtains

$$[M] \{\ddot{u}\} - \left(\frac{q_\infty}{V_\infty} \cdot 2 [Q] [A]^{-1} [E]\right) \{\dot{u}\} + \left([K] + q_\infty \cdot 2 [Q] [A]^{-1} [D]\right) \{u\} = \{0\} \tag{3.50}$$

This is where one of the solution methods mentioned in section 2.2 has to be applied. The most suitable one for the case being studied is the P-Method because it allows to use the same aerodynamic model as for the static coupling case. It is true that this method gives a quasi-static solution and not an unsteady one but considering unsteady regime would increase a lot the complexity and it would be truly beyond the scope of this work.

Therefore, the P-Method is chosen. If the system is to be solved as an eigenvalue problem, there can not be three different vectors multiplying each main matrix in the equation. So, introducing the eigenvector $\bar{u}$ the three vectors become

$$\begin{aligned} \{u\} &= \{\bar{u}\} e^{pt} \\ \{\dot{u}\} &= p \{\bar{u}\} e^{pt} \\ \{\ddot{u}\} &= p^2 \{\bar{u}\} e^{pt} \end{aligned} \tag{3.51}$$

where t is the time and p is a parameter whose real part will allow to analyze the stability of the system.

Taking a look at the previous equation, if the real part of p is negative or equal to zero the system's response is stable while if it is positive the response of the system is unstable. That is why the flutter condition will be studied from the sign of the parameter p.

Applying these changes to Equation 3.50 and tacking common factor of vector $\{\bar{u}\}$ the final equation for the dynamic coupling case is obtained.

$$\left(p^2 [M] + p [C_a] + [K_a]\right) \{\bar{u}\} e^{pt} = \{0\} \tag{3.52}$$

In this equation matrix $[M]$ is the same mass matrix stated previously in the section and matrices $[C_a]$ and

$[K_a]$ are:

$$\begin{aligned}[C_a] &= -\frac{q_\infty}{V_\infty} \cdot 2\,[Q]\,[A]^{-1}\,[E] \\ [K_a] &= [K] + q_\infty \cdot 2\,[Q]\,[A]^{-1}\,[D]\end{aligned} \tag{3.53}$$

Naturally, the exponential function in Equation 3.52 can never be zero so it can be simplified. The eigenvalue problem becomes then

$$\left(p^2\,[M] + p\,[C_a] + [K_a]\right)\{\bar{u}\} = \{0\} \tag{3.54}$$

The idea to solve this equation is finding the value of p given different values of the freestream velocity V_∞. The equivalent stiffness and damping matrices of the equation depend on V_∞ and that is why the values need to be predefined.

The last equation, the one that characterizes the dynamic system, can be written in matrix form thus extended to a matrix system of equations. It states

$$\left(\left[\bar{K}\right] - \lambda\left[\bar{M}\right]\right)\{\bar{v}\} = \{0\} \tag{3.55}$$

where λ is the eigenvalue p with opposite sign and the other components are:

$$\{\bar{v}\} = \left\{ \begin{array}{c} \bar{u} \\ \dot{\bar{u}} \end{array} \right\} \equiv \left\{ \begin{array}{c} \bar{u} \\ p\,\bar{u} \end{array} \right\} \tag{3.56}$$

$$\left[\bar{M}\right] = \left[\begin{array}{cc} C_a(V_\infty) & M \\ -\mathbb{1} & 0 \end{array} \right] \qquad \left[\bar{K}\right] = \left[\begin{array}{cc} K_a(V_\infty) & 0 \\ 0 & \mathbb{1} \end{array} \right] \tag{3.57}$$

The effective stiffness and mass matrices are not symmetric and $\mathbb{1}$ is the identity matrix of dimensions $N_{DOF} \times N_{DOF}$.

If one divides this matrix system of equations into two separated equations to prove that its formulation is consistent, the equations that appear are

$$\left(\left[\begin{array}{cc} K_a(V_\infty) & 0 \\ 0 & \mathbb{1} \end{array} \right] + p \left[\begin{array}{cc} C_a(V_\infty) & M \\ -\mathbb{1} & 0 \end{array} \right] \right) \left\{ \begin{array}{c} \bar{u} \\ p\,\bar{u} \end{array} \right\} = \left\{ \begin{array}{c} 0 \\ 0 \end{array} \right\} \tag{3.58}$$

$$\begin{cases} (K_a + p\,C_a)\,\bar{u} + p^2\,M\,\bar{u} = 0 \\ p\,\mathbb{1} - p\,\mathbb{1} = 0 \end{cases} \tag{3.59}$$

The second equation is an identity to prove that the system is well formulated so the important result is found in the first one, which extended is the same as Equation 3.54:

$$\left(p^2\,[M] + p\,[C_a] + [K_a]\right)\{\bar{u}\} = \{0\}$$

Therefore the values to study the flutter condition by solving the equation will be the first half DOFs, the ones that come from the solution of the first equation in system 3.58. In there, p is the eigenvalue sought and

$\{\bar{u}\}$ the effective displacements' eigenvector. The idea is to study the system's stability via a plot of the real part of p versus the freestream velocity, in order to find for which velocity and mode the real part of p goes from a negative value (stable) to a positive value (unstable). This point corresponds to a flutter condition.

Chapter 4

Computational Approach

Once the theory is exposed, it is time to adapt the problem in order to solve it via computational methods. This chapter defines the wing discretization and the aerodynamic and structural computational coupling methods.

Appendices A and B develop the FEM, the HVM and the VLM, three methods that are necessary to obtain the matrices that determine the modal analyses carried out in the coupling sections.

4.1 Discretization of the Domain

In this section, the wing mesh is created according to the theory developed in the Wing Geometry part. The number of elements in every direction, the necessary structural and aerodynamic points and parameters and the connectivity matrices are among the most important issues to solve.

Although the mesh is flat, the problem will be treated as 3D for the sake of generality. At first, the material parameters and general dimensions are defined. The wingspan and the root chord are the ones in Equation 3.1 while the material properties are exposed in Tables **1** and **3**.

Then, since one of the objectives of the project is to carry out a parametric study, it is better to define the TR, SW and AR after the general dimensions. The TR and the SW are defined directly by putting a number there. Once decided the values for both, the tip chord and the wing surface can be computed with

$$\begin{aligned} c_t &= c_r\, TR \\ S_w &= \frac{(c_r + c_t)\cdot b}{2} \end{aligned} \tag{4.1}$$

since the wing has a trapezoidal planform and the subscripts t, r and w stand for *tip*, *root* and *wing*, respectively.

Consequently, the AR is directly computed using Equation 3.6:

$$AR = \frac{b^2}{S_w} \tag{4.2}$$

Being all these input data chosen and defined, it is time to move on to the mesh generation. To begin with, the number of elements in the XY plane is decided:

$$\left.\begin{aligned} x_{el} &= 10 \\ y_{el} &= 16 \end{aligned}\right\} \longrightarrow N_{el} = x_{el} \cdot y_{el} = 160 \tag{4.3}$$

Therefore, the total number of nodes is

$$\left.\begin{aligned} x_{nod} &= x_{el} + 1 = 11 \\ y_{nod} &= y_{el} + 1 = 17 \end{aligned}\right\} \longrightarrow N_{nod} = x_{nod} \cdot y_{nod} = 187 \tag{4.4}$$

Because the problem is 3D, each node has 6 DOFs so the mesh has $N_{DOF} = 6N_{nod} = 1122$.

What is next is the computation of the coordinates' matrix. This step is arguably the most important, and its development is presented below.

- The element widths in the x and y directions are calculated:

$$\begin{aligned} \Delta x &= \frac{c(y)}{x_{el}} \\ \Delta y &= \frac{b}{y_{el}} \end{aligned} \tag{4.5}$$

  Notice that throughout the x-axis Δx depends on the chord length in that position. It is directly affected by the TR.

- The chord length in every y position can be expressed by the equation of a straight line:

$$c(y) = \frac{(c_t - c_r)}{b} y + c_r \tag{4.6}$$

- Then, the coordinates are also affected by the SW. As explained in subsection 3.1.2, the SW is the angle between the y-axis and the quarter-chord line of the wing. This way the computation of the quarter-chord coordinate along y gives the expression:

$$c_{25}(y) = \frac{1}{4} c_r + y \cdot \tan(SW) \tag{4.7}$$

- With these two vectors, running a double for loop through the x and y nodes, the coordinates of each node are obtained:

$$\begin{aligned} X(i,j,1) &= c_{25}(y) - \frac{1}{4} c(y) + (i-1)\,\Delta x \\ X(i,j,2) &= (j-i)\,\Delta y \end{aligned} \tag{4.8}$$

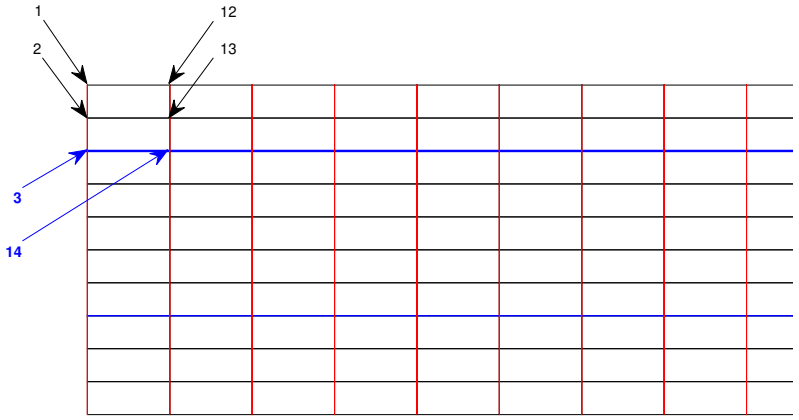

Figure 25 First plate, LE spar, and rib elements' nodes to define the connectivities.

The variables i and j refer to the node number in the x and y positions thus they go from 1 to 11 and from 1 to 17, respectively.

- Finally, the positions of the two spars, the LE and the TE ones, and of the ribs are to be defined. It is decided that the LE spar will be at 20% chord, the TE spar at the 70% and the ribs will go through all the chord positions, being 17 in total.

Once the coordinates are defined, it only remains the computation of the connectivity matrices, also a very important part. As the mesh is structured it is not a difficult step.

- For the quadrilateral elements the nodes are ordered counterclockwise so, for example, the connectivity of the first element will look like [1 2 13 12]. Figure **25** represents the connectivities for the first plate, the first LE spar and the first rib elements.
- For the two-noded spar elements the connectivity matrix is even simpler, it is only necessary to add 11 nodes, because they go in the y direction. The first element of the TE spar will look like [3 14].
- For the two-noded rib elements the connectivity follow the sample principle as the spars but the nodes are distributed along the x direction, bring the first element of the tip rib, for example, [177 178].

As a final comment, another vector is needed for the aerodynamic calculations, the collocation points' coordinates. As it is in the middle of the panel, the computation consists of finding the quarter and three-quarter chord points in every y position of the nodes and then find the mean value in every element. For example, for the first element, which is between the first and second ribs, the collocation point will look like

$$\begin{aligned} X_{coll,1}(el=1,1) &= \frac{X(i=1,j=1,1)+X(i=1,j=2,1)}{2} + \frac{3}{4}\frac{\Delta x(i=1,j=1)+\Delta x(i=1,j=2)}{2} \\ X_{coll,1}(el=1,2) &= \frac{X(i=1,j=1,2)+X(i=1,j=2,2)}{2} \end{aligned} \tag{4.9}$$

where the first coordinate is the x and the second the y.

Figure **26** shows the mesh representation including the normal vectors placed at the collocation points of

each element. All the normal vectors have the components [0 0 1] because the mesh is flat.

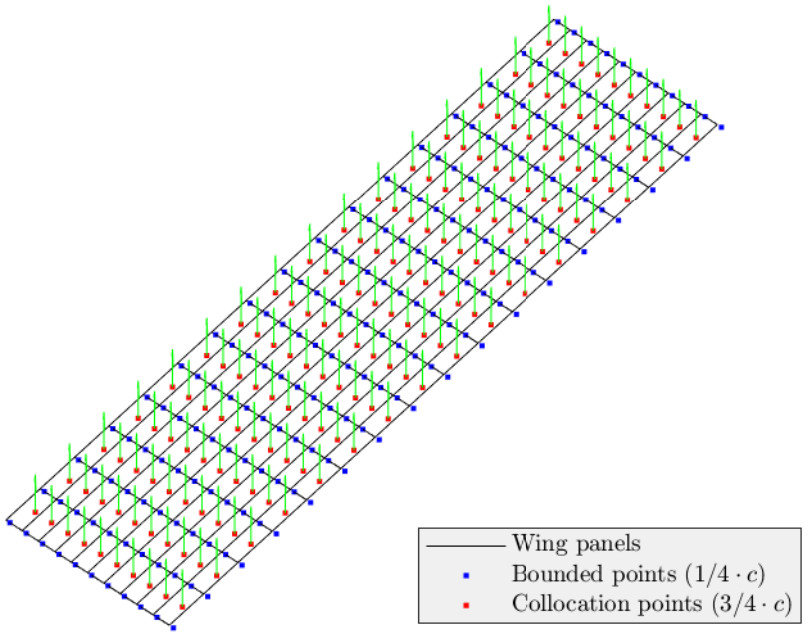

Figure 26 Discretized mesh of the semi-wing including the aerodynamic bounded and collocation points together with the normal vectors in these last.

4.2 Coupling Systems

After the aerodynamic and structural coupling was presented in section 3.4, it is time to explain how the theories can be extended to computational language. This section provides the development of the necessary matrices to formulate the static and dynamic systems so that the flutter condition can be properly studied. Apart from that, it is the last step before presenting the results of the study, the computational development finishes at the end of the section.

4.2.1 Static coupling system

In subsection 3.4.1 the matrix system of equations obtained was the one in Equation 3.39:

$$\left([K] + q_\infty \cdot 2\,[Q]\,[A]^{-1}\,[D]\right)\{u\} = \{0\}$$

As stated in the corresponding subsection, it is and eigenvalue problem in which the eigenvalues and eigenvectors are q_∞ and $\{u\}$ while the matrices that complete the system are $[K]$ and $\left(-2\,[Q]\,[A]^{-1}\,[D]\right)$.

The stiffness matrix appears when solving the FEM for all the elements in the wing; skin, spars and ribs.

On the other hand, the aerodynamic matrix is a combination of three different matrices; the inverse of the influence coefficients, obtained by solving the VLM, the one that relates the circulations vector to the lift, which is $[Q]$ and finally $[D]$ that connects each AoA to the vertical displacements vector.

Therefore, the computational implementation of matrices $[D]$ and $[Q]$ is to be explained below.

- **$[D]$:** It must comply with Equation 3.24, $\{\alpha\} = [D]\{u\}$, and the process to follow includes the steps below.
  - Start a *for* loop which includes all the elements e of the mesh.
  - Then, for each element the panel width (in the x direction) is computed with the expression[1]

$$d = \frac{X(T_n(e,2),1) + X(T_n(e,3),1)}{2} - \frac{X(T_n(e,1),1) + X(T_n(e,4),1)}{2} \tag{4.10}$$

  - Last but not least, for each node in the element, according to Equation 3.30, the corresponding contribution is

$$\begin{aligned} D(e, 6\,T_n(e,1) - 3) &= \frac{1}{2\,d} \\ D(e, 6\,T_n(e,4) - 3) &= \frac{1}{2\,d} \\ D(e, 6\,T_n(e,2) - 3) &= -\frac{1}{2\,d} \\ D(e, 6\,T_n(e,3) - 3) &= -\frac{1}{2\,d} \end{aligned} \tag{4.11}$$

    where e refers to the element that the loop is analyzing and T_n to the connectivities matrix. The AoA is being related to the vertical displacement vector, which corresponds to the third DOF, and that is why the column index of the matrix subtracts 3 units to the product of the connectivities matrix and 6, which is the number of DOFs per node.

- **$[Q]$:** It must comply with Equation 3.31, $\{f\} = [Q]\{\Gamma\}$, in which the external force refers to the lift. The steps to follow to fill the matrix are presented below.
  - As for the first matrix, it is necessary to start a *for* loop that goes through all the elements e of the mesh.
  - Next, the panel's length in the span direction (y axis) is computed. The expression to do so is

$$\Delta y = \frac{X(T_n(e,4),1) + X(T_n(e,3),1)}{2} - \frac{X(T_n(e,1),1) + X(T_n(e,2),1)}{2} \tag{4.12}$$

  - Finally, for each node in the element, according to Equations 3.34 and 3.35 the contribution to the matrix is

$$\begin{aligned} Q(I_{dof}, e) &= Q(I_{dof}, e) + \frac{\Delta y}{4} \\ Q(I_{dof}, e^*) &= Q(I_{dof}, e^*) + \frac{\Delta y}{4} \end{aligned} \tag{4.13}$$

    where e refers to the element being analyzed, I_{dof} to the DOFs in which lift actuates, that is to

[1] The element nodes are ordered counterclockwise, see Figure **19** to remember.

say, the vertical displacement DOF of the four nodes that make up the element and e^* to the adjacent element closer to the LE thus it is not taken into account when studying LE panels.

Now that the matrices are found the modal analysis can be run. The eigenvalue problem is represented by Equation 3.39 and the steps to follow to write the code are the following.

- First of all the number of eigenvalues is set. In this case this number is 18, providing a strong solution of the system.
- Then, the four matrices that take part in the equation are defined, these being
  - Stiffness matrix $[K]$
  - Influence coefficients matrix $[A]$
  - Displacements coupling matrix $[D]$
  - External force coupling matrix $[Q]$
- Next, one of the most important steps is to apply the boundary conditions. As the body is a semi-wing the left-border nodes are clamped, similar to a cantilever beam. This way, all the DOFS of these nodes will be zero. The most efficient way is to create a short function that returns two vectors, one with the restricted DOFs and the other one with the free DOFs.
- The four matrices are reduced in dimension, only the free DOFs take part in the resolution[2]. Apart from that, the aerodynamic and coupling matrices are multiplied so to from the equivalent to the mass matrix in a structural eigenvalue problem (see 3.22). It looks like

$$[M_f] = -2\,[Q]\,[A]^{-1}\,[D] \tag{4.14}$$

  where the subscript f refers to the word *free*, meaning that the matrix shows only the free DOFs indices, and the negative sign is placed so the eigenvalues are obtained with the correct sign[3]
- Finally, a function that returns the eigenvalues q_∞ and eigenvectors $\{u\}$ of the 18 eigenmodes is run. Inside the function, the modes are solved and ordered from smallest to largest in terms of the dynamic pressure.

Additionally, the modes can be plotted so to create a more visually appealing representation. Moreover, it will be important to know which mode activates the divergence condition because it is not the same to deal with it in a bending mode than in a twist one.

One methodology that allows differentiating between these two types of deformation consists of studying the values of the eigenvectors $\{u\}$. The bending eigenmodes activate mainly the vertical displacement DOFs (in the z axis), which are the same for all nodes in the same airfoil section, while the twist eigenmodes require of studying an angle. Assuming small deformation, the twist along the wingspan (y-axis) can be computed with

[2]The eigenvector positions of the restricted DOFs will be zero.
[3]For further explanation regarding the sign issue see subsection 3.4.1.

the expression

$$\theta_y = \frac{u_{z_{LE}} - u_{z_{TE}}}{c(y)} \tag{4.15}$$

where the LE corresponds to the first node of the chord and the TE to the last one. Apart from that, when the TR and SW are implemented, the chord is not constant along the span and that is why it depends on y.

An accurate study of the results is presented in the next section.

4.2.2 Dynamic coupling system

The dynamic coupling system is an extension of the static system, and two new matrices appear. The expression that characterizes the system is presented in Equation 3.54:

$$\left(p^2 [M] + p [C_a] + [K_a]\right) \{\bar{u}\} = \{0\}$$

A whole new term is added, the one characterized by the mass matrix $[M]$. Then, the damping term is represented by the damping aerodynamic matrix $[C_a]$ and the stiffness term by $[K_a]$, a combination of the structural stiffness matrix $[K]$ and another one containing aerodynamic elements. For further detail see subsection 3.4.2.

In this case, the eigenvalue is p and the eigenvector is $\{\bar{u}\}$. To solve the system, the previous equation is extended to a matrix system of equations, the one represented by Equation 3.58:

$$\left(\begin{bmatrix} K_a(V_\infty) & 0 \\ 0 & \mathbb{1} \end{bmatrix} + p \begin{bmatrix} C_a(V_\infty) & M \\ -\mathbb{1} & 0 \end{bmatrix} \right) \begin{Bmatrix} \bar{u} \\ p\,\bar{u} \end{Bmatrix} = \begin{Bmatrix} 0 \\ 0 \end{Bmatrix}$$

As explained previously, there are two new matrices. One is the mass matrix $[M]$, which is computed using the FEM like the stiffness one and the other is matrix $[E]$, which relates the structural displacement of the elements in direction z to the displacements of all the nodes. This last matrix is obtained following the steps below.

- **$[E]$:** It must comply with Equation 3.44, $\{\dot{u}_z\} = [E]\{\dot{u}\}$, in which the transformation is from the vertical structural velocity of the panel to the vector containing all the velocities of the DOFs, not only the vertical one in the z direction.
  - Once again, the first step is to start a *for* loop that goes through all the elements e of the mesh.
  - Then, the only thing needed is to evaluate the shape function of a quadrilateral element in the collocation point because it is the point where the structural velocity is applied. Taking a look at Figure **24**, these coordinates are

    $$\xi_c = 0.5 \qquad \eta_c = 0$$

    and the shape function is defined in Equation 3.46, where the parameters a and b are detailed in Appendix A.2.3.

Being the matrix defined it is time to explain how the system of equations is solved computationally. The steps to follow are:

- The number of eigenvalues is the first issue to set. It needs to be the same as in the static coupling so to analyze the modes that activate flutter and its corresponding divergence velocities. Therefore, the number is set to 18.
- A freestream velocity vector is also necessary to define, for each velocity in this vector the modal problem will be solved, providing, at the end, the flutter envelope plot[4].
- Then the mass, damping and stiffness matrices are defined, these being
  - Mass matrix $[M]$
  - Damping matrix $[C_a] = -\frac{q_\infty}{V_\infty} \cdot 2\,[Q]\,[A]^{-1}\,[E]$
  - Stiffness matrix $[K_a] = [K] + q_\infty \cdot 2\,[Q]\,[A]^{-1}\,[D]$
- Next, the extended matrices are written down
  - Mass extended matrix $\left[\bar{M}\right] = \begin{bmatrix} C_a(V_\infty) & M \\ -\mathbb{1} & 0 \end{bmatrix}$
  - Stiffness extended matrix $\left[\bar{K}\right] = \begin{bmatrix} K_a(V_\infty) & 0 \\ 0 & \mathbb{1} \end{bmatrix}$
- The system is solved, giving a vector of complex numbers that represent the eigenvalues λ. Because they are complex, the real and imaginary parts are separated, giving

$$\begin{aligned} p_R &= Re\,(-\lambda) \\ p_I &= Im\,(-\lambda) \end{aligned} \tag{4.16}$$

  Moreover, the eigenvectors wanted are the first half of the extended ones (see the definition of the system in 3.58), the first half corresponds to the values of $\bar{u}$ and the second half to $p\,\bar{u}$:

$$\Phi_p = \bar{v}\,(1 : N_{DOF}) \tag{4.17}$$

Once the modal system is solved for all the freestream velocities defined, the flutter velocity can be determined. It is the final part of the code, the ultimate result sought. The vectors needed to build the graph are the real eigenvector part $\{p_R\}$ and the freestream velocity $\{V_\infty\}$ vectors.

Eighteen curves will appear in the flutter plot, one for each mode. The flutter velocity is found when a curve changes from negative to positive sign. At the point that it crosses a horizontal line placed at $p_R = 0$, the condition is satisfied. There may be more than one flutter velocities, the instability can appear in a bending or a twist eigenmode, for example. However, the most critical condition must be picked, it will be the first to make the wing unstable, thus the most dangerous one.

[4]The idea, for each mode, is to set velocities up to the double of its divergence velocity. Flutter is an instability so it should appear before divergence.

It is important to know that finite discontinuities may also appear (see Figure **27**). It sometimes happens because the eigenmodes do not always come out ordered. These discontinuities should not be misunderstood as flutter conditions. So to avoid wondering whether the plot is well analyzed or not, one can interpolate and choose, for each velocity, the maximum value of the eigenvalues vector $\{p_R\}$ (see Figure **33**). This way, the most critical flutter velocity will be found, together with the corresponding eigenmode.

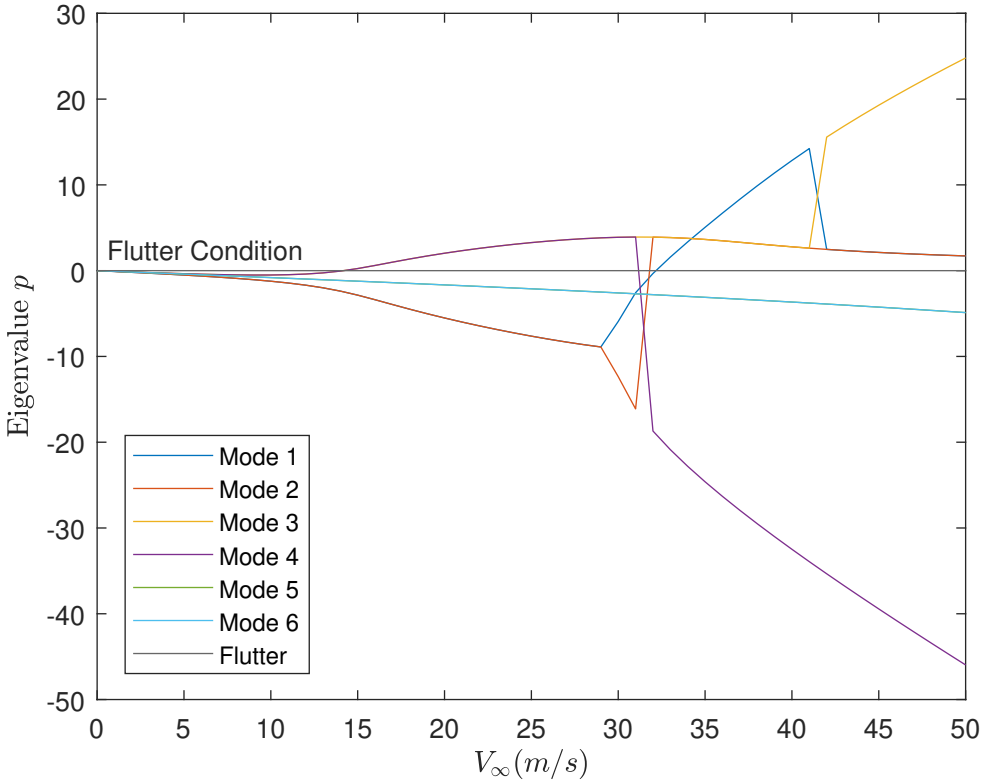

Figure 27 Flutter plot discontinuities of modes 1-6 for the original wing case.

Chapter 5

Results

The Result's chapter looks forward to studying the behavior of the planar wing when withstanding static aerodynamic loads. On the one hand, the dynamic response of the wing is analyzed, while, on the other hand, the solution is extended to observe the flutter instability. The parameters which trigger this instability and, thus, affect directly the wing's performance are to be found and modified.

5.1 Dynamic Response of the Wing

The first results of the behavior of the wing are the eigenmodes. These are obtained when solving the static coupling expression exposed in Equation 3.39. The number of modes was set to 18 previously and they are depicted, together with their eigenvalues, in Figures **28**, **29** and **30**.

Before analyzing their deformations, an initial filter is established so not to consider the wrong modes. It is related to the eigenvalues q_{inf}. Notice that for the first six modes the dynamic pressures are negative, meaning that these are modes that do not activate using the aerodynamic model implemented in this project.

This happens because, in the static modal analysis, the pure bending motion does not create lift, it is not affected by the aerodynamic model. Not only the first six modes, with the negative eigenvalue but also the other bending modes are not affected, from 15 to 18.

To prove this last statement a simple calculation can be made. According to Equation 3.30, the angles of attack of each panel are obtained by multiplying matrix $[D]$ by the eigenvectors of each mode. By doing so in the code, Tables **5** and **4** show the modes which are activated by the aerodynamic model (twisting deformation), like 8 and 10, and the ones that are not (bending deformation), like 5 and 6.

After all, it is important that the value of the dynamic pressure is positive because it carries with him a physical interpretation and the divergence velocity of the mode is to be computed with this value. The expression is simple:

$$V_{div} = \sqrt{\frac{2q_\infty}{\rho}} \tag{5.1}$$

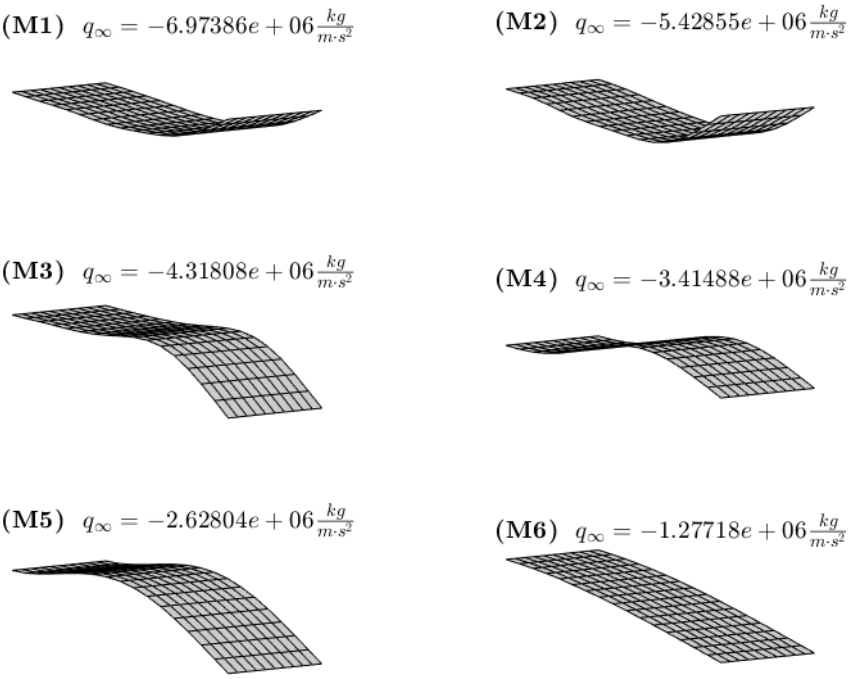

Figure 28 Representation of eigenmodes 1 to 6, together with their corresponding eigenvalues.

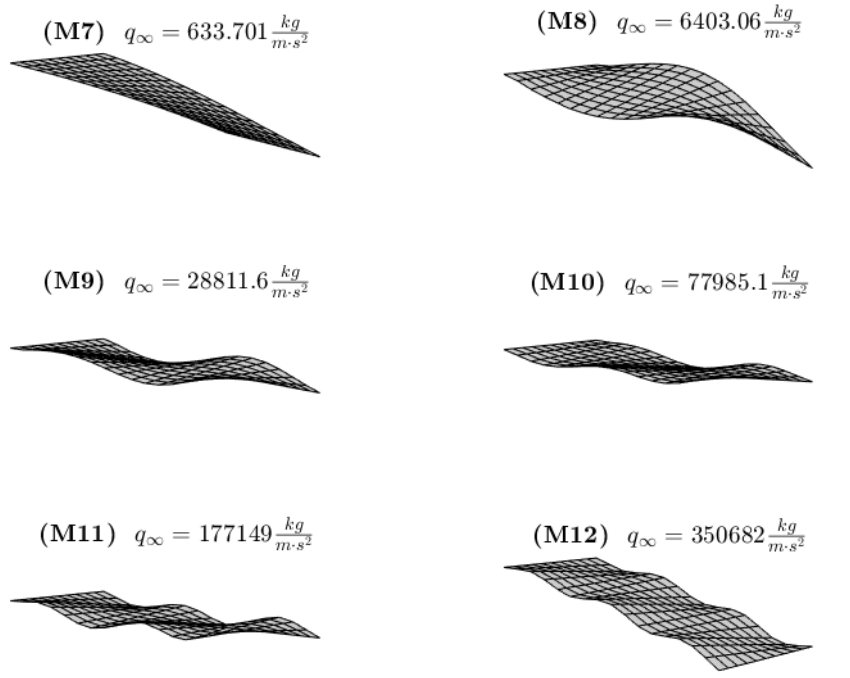

Figure 29 Representation of eigenmodes 7 to 12, together with their corresponding eigenvalues.

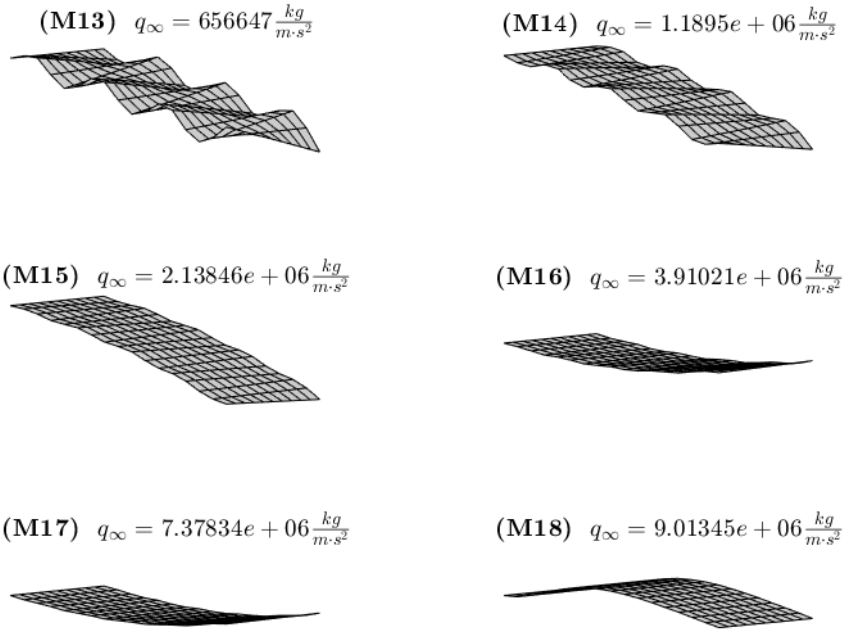

Figure 30 Representation of eigenmodes 13 to 18, together with their corresponding eigenvalues.

Table 4 Maximum ‖AoA‖ value of the bending eigenmodes.

Eigenmode	Max ‖AoA‖ (º)	Activated
1	0.1243	No
2	0.1355	
3	0.1319	
4	0.1010	
5	0.0096	
6	0.0366	
15	0.4874	
16	0.2612	
17	0.1387	
18	0.1055	

Table 5 Maximum ‖AoA‖ value of the twisting eigenmodes.

Eigenmode	Max ‖AoA‖ (º)	Activated
7	5.9770	Yes
8	6.5792	
9	4.3885	
10	2.4773	
11	2.5134	
12	1.6915	
13	1.8759	
14	1.3021	

Table 6 Flutter condition for the original wing shape.

V_{flut} (m/s)	Eigenmode	Type of Motion
14.1701	3	Twisting

The density ρ corresponds to the freestream air density and it depends on the flying altitude. In order not to make the work more difficult, the sea level condition is chosen, being the air density $\rho = 1.225\, kg/m^3$.

Finally, a last classification can be made. Flutter arises, in this case, only from twisting motion, so to know which modes will not affect the instability it is necessary to classify the modes in bending or twist. This will be made by applying Equation 4.15 for the twist or by adding all the vertical displacements at fixed y nodes and dividing the sum by the chord for bending. Figures **31** and **32** plot the nodes that correspond to bending and the modes that correspond to twist, respectively.

As a last comment, according to the results in Tables **4** and **5**, modes 15 and 16 are in the middle of bending and twisting deformation. It is clear that in Figure **30** a bit of twist is appreciated in these modes, although the predominant motion is bending.

5.2 Flutter Instability

After presenting and discussing the results of the static coupling case it is time to move on to the dynamic coupling. In this case, the eigenvalues that result of the modal analysis do not have physical meaning in but they are a means to obtain the flutter velocity.

For the original wing shape ($TR = 1$, $SW = 0°$ and $AR = 4$), the flutter plot is represented in Figure **33** and the velocity together with the eigenmode that triggers the instability are exposed in Table **6**.

It is important to remark that in the dynamic coupling system, the aerodynamics do not depend only on the wing twist. Bending contributes to the flutter instability because this phenomenon also depends on the vertical velocity of the panel, as seen in Equation 3.50. Therefore, both the bending and twisting motion can generate lift by themselves and trigger the flutter instability.

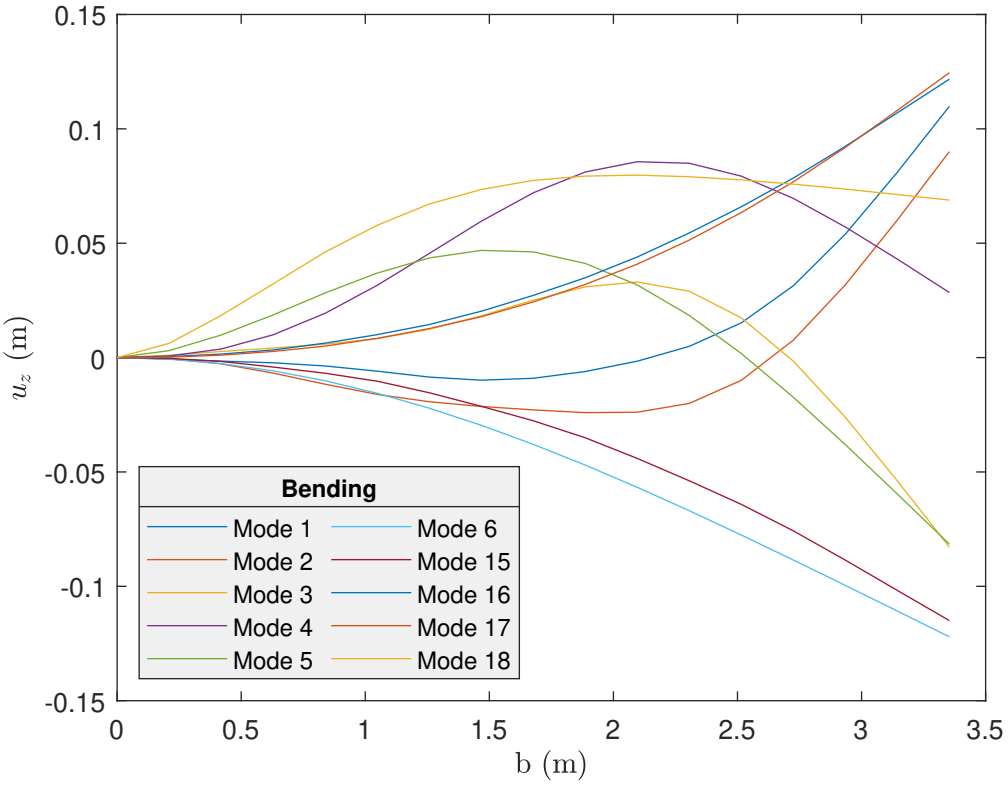

Figure 31 Modes that correspond to bending motion.

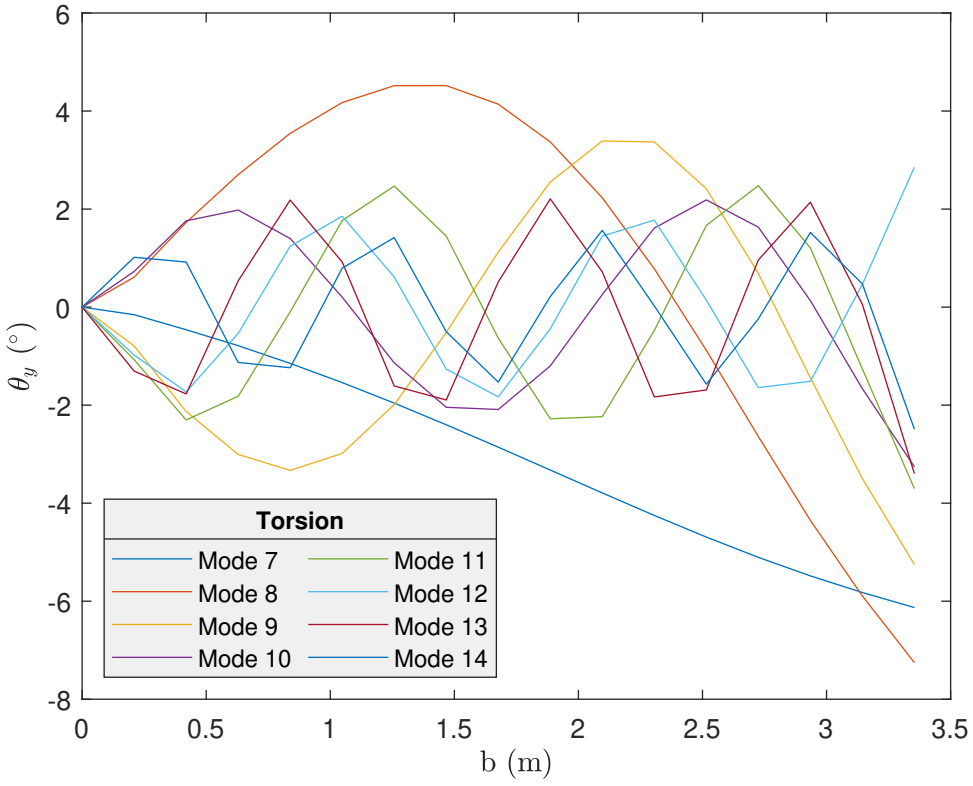

Figure 32 Modes that correspond to twisting motion.

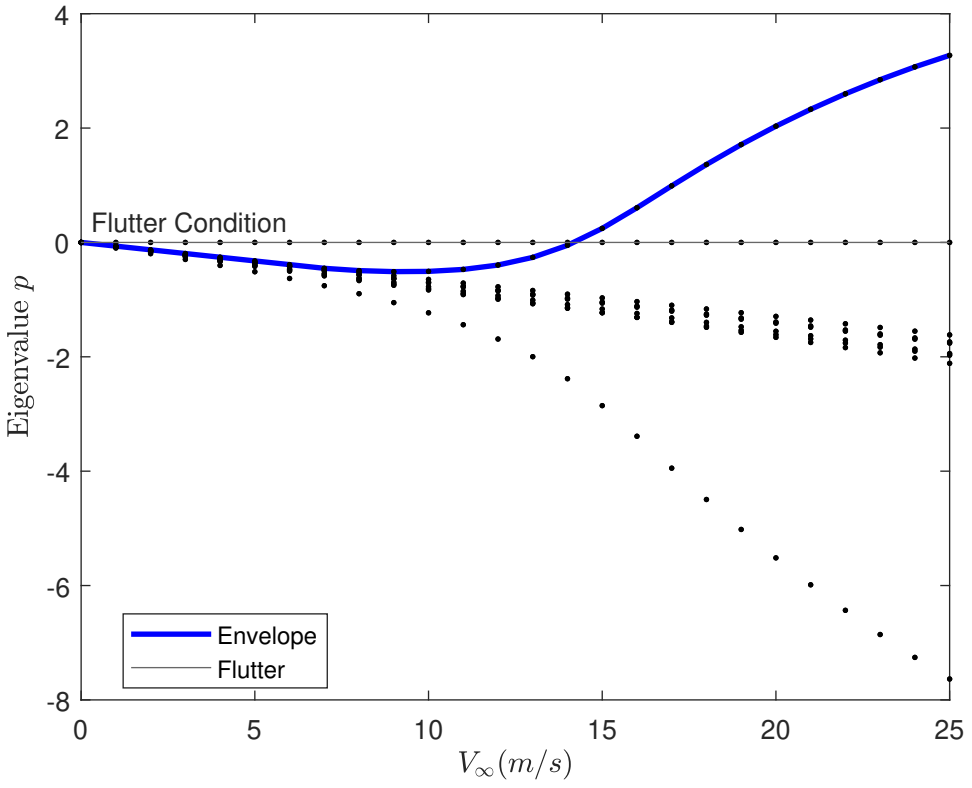

Figure 33 Mode plotting and flutter condition for the original wing shape ($TR = 1$, $SW = 0°$ and $AR = 4$).

Table 7 TR and SW values selected to study the flutter condition.

TR	0.1	0.2	0.3	0.4	0.5	0.6	0.7	0.8	0.9	1
SW (°)	5		10	15	20	25	30	35	40	

In the next section, a parametric study will be carried out, so to study the effects of TR, SW, AR and additional point masses at different nodes on the flutter condition.

5.3 Parametric Study

This section provides a deeper study into the different parameters that can affect the flutter condition. These parameters are the taper ratio (TR), the sweep angle (SW), the aspect ratio (AR), the three explained in subsection 3.1.2. Moreover, the addition of a point mass at different nodes will also be studied because the weight is critical in the aeronautics field and a more realistic approach will be made.

5.3.1 Taper ratio & Sweep angle

To begin with, TR and SW are analyzed together. Figure **34** shows the surface plot representing the flutter velocity for each combination of the two parameters. The values studied are summarized in Table **7**.

The tendency followed by the 3D plot can be summarized in the following items:

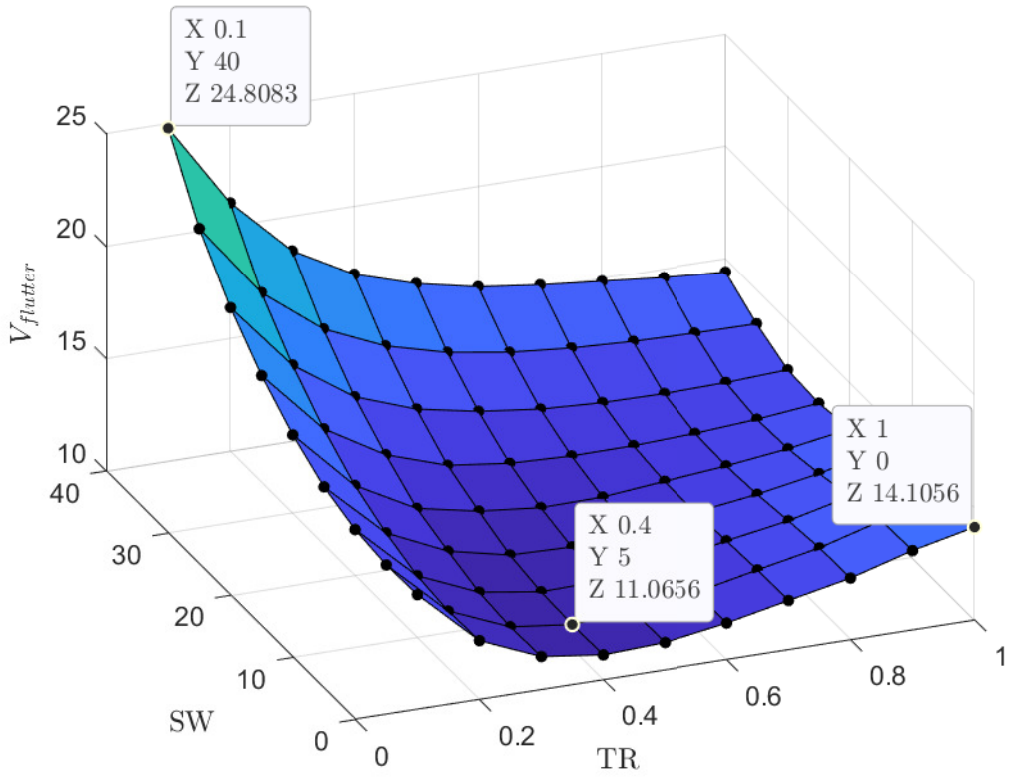

Figure 34 Flutter velocity conditions for different TR and SW combinations.

- For high TR values, from 0.6 to 1, and for low SW angles, from 0° to 15°, the flutter speed is reduced when decreasing the TR and increasing the SW.
- For low TR values, from 0.1 to 0.6, and for high SW angles, from 15° to 40°, the flutter speed increases considerably, especially when getting to the most critical parameters values (maximum SW and minimum TR).
- The original wing shape, with $TR = 1$ and $SW = 0°$, is not the most critical condition for the flutter speed.
- For intermediate values of both parameters, the variation of the flutter speed is not very significant. Real wings do not tend to have so little TR and high AR like 0.1 or 40° so the influence is not very high.

In Table **7** the most critical flutter conditions, both the maximum and minimum, are compared to the original wing shape condition.

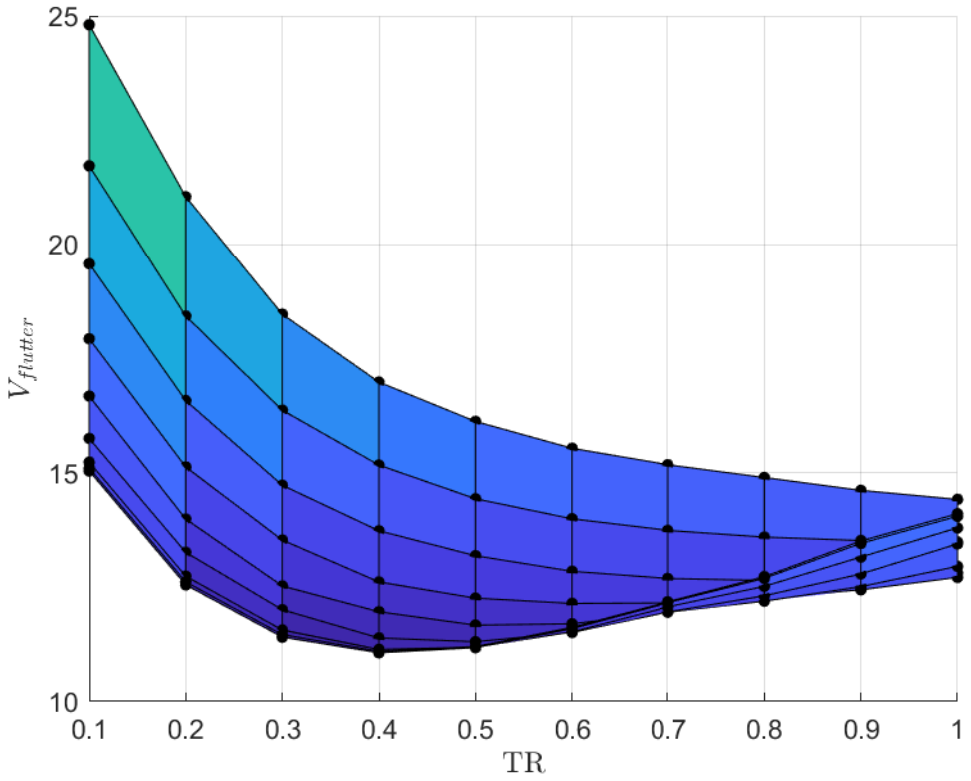

Figure 35 Flutter speed vs TR for constant SW values (side view of the 3D surface plot).

Table 8 Maximum and minimum flutter velocities, obtained modifying the TR and the SW, compared to the original one.

	TR	**SW (º)**	$V_{flutter}$ **(m/s)**	% $V_{flutter}$ **Original**
Min	0.4	5	11.0656	78.5
Original	1	0	14.1056	100
Max	0.1	40	24.8083	175.9

Then, Figures **35** and **36** try to give a detailed view on the flutter condition by modifying the parameters separately.

The two behaviors are quite opposite. While the TR effect is that of increasing the flutter velocity when reducing its value, the SW effect increases the instability velocity when a higher angle is implemented.

In both cases there is this change in the behavior just mentioned, for the highest values of TR and the lowest of SW. The difference is small though, like the flutter speed.

As a comment regarding these first parameters plotted, TRs higher than 1 and negative or higher than 40° SW angles are not considered because they are not common in aeronautics thus the results would not be accurate neither realistic.

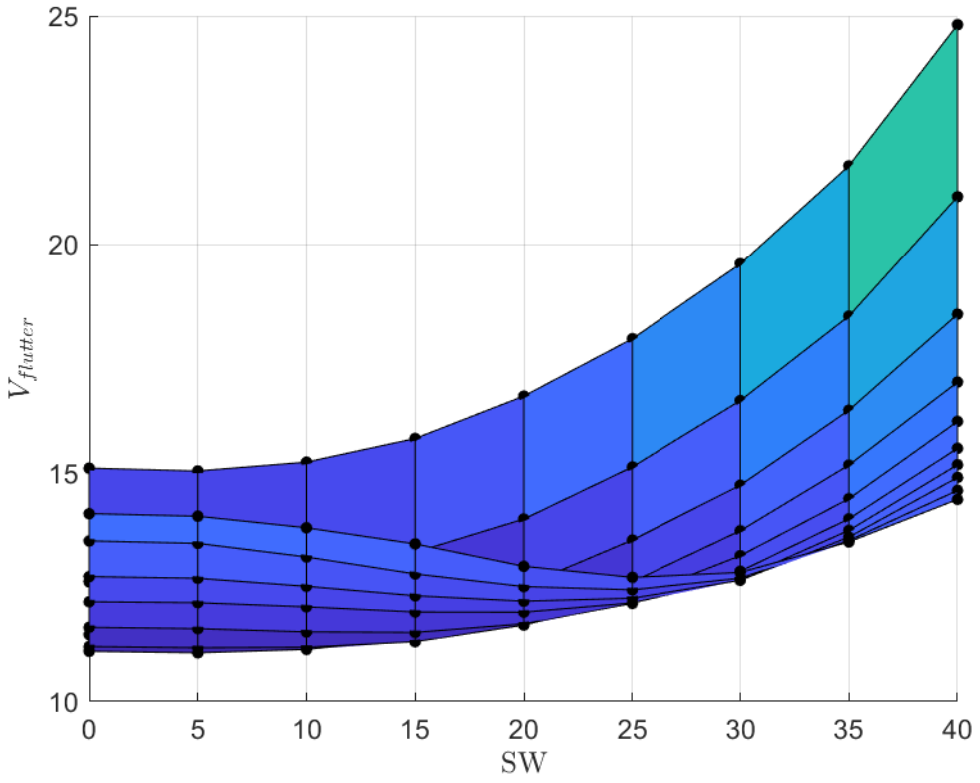

Figure 36 Flutter speed vs SW for constant TR values (side view of the 3D surface plot).

Table 9 Semi-span and root chord values selected to study the flutter condition.

b (m)	2.0124	2.3478	2.6832	3.0186	**3.3540**	3.6894	4.0248	4.3602	4.6956
c_r **(m)**	0.5028	0.5866	0.6704	0.7542	**0.8380**	0.9218	1.0056	1.0894	1.1732
% Original	60	70	80	90	100	110	120	130	140

5.3.2 Aspect ratio

Now, the second parameter studied is the AR. The idea is to choose different dimensions of the wing span b and the root chord c_r so that the AR is modified. The TR and the SW are kept as for the original case so that they do not interfere in the solution.

Before presenting the results, it is important mentioning that the AR can be the same for two different combinations of span and chord. Therefore, it will not only be important the value of the AR but also the wing planar shape.

The values selected to carry out this study case are presented in Table **9** while the 3D surface plot corresponds to Figure **37**.

Looking at the graph in detail several preliminary conclusions can be drawn:

- The flutter speed increases when reducing the span and increasing the root chord, that is to say, when the AR decreases.

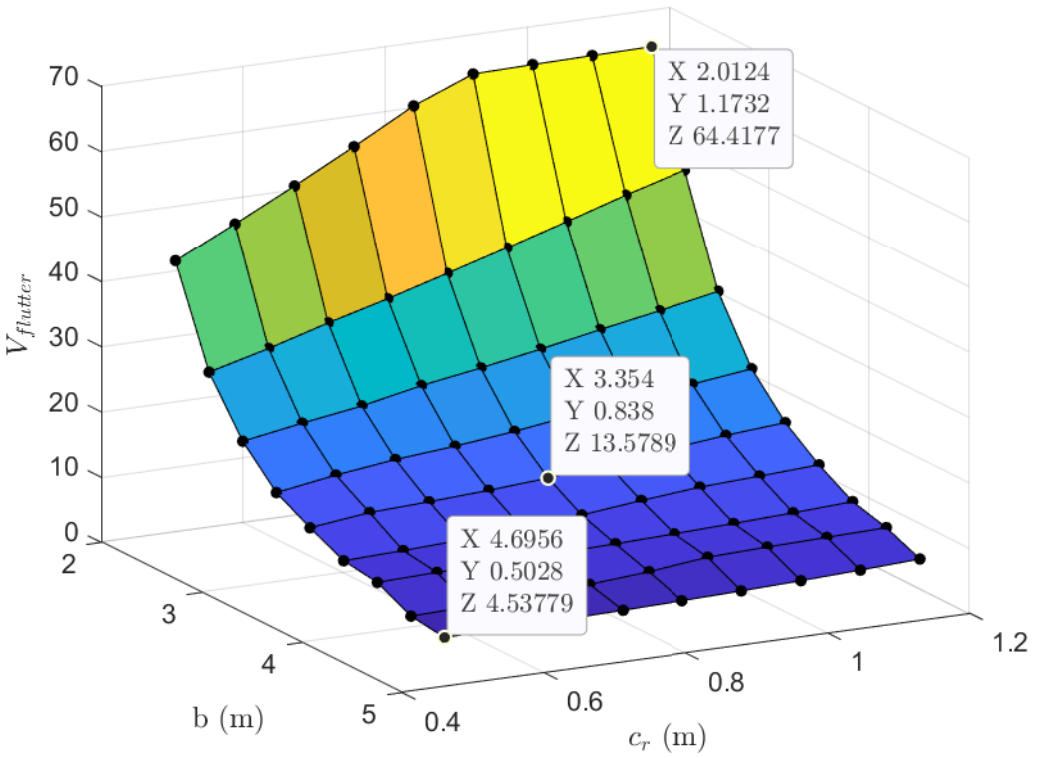

Figure 37 Flutter velocity conditions for different percentages of b and c_r thus different AR values.

Table 10 Maximum and minimum flutter velocities, obtained modifying b and c_r, compared to the original one.

	b (m)	c_r **(m)**	$V_{flutter}$ **(m/s)**	% $V_{flutter}$ **Original**
Min	4.5378	0.5028	4.6956	34.6
Original	3.354	0.838	13.5789	100
Max	2.0124	1.1732	64.4177	474.4

- For a constant root chord, the increase in the flutter speed when reducing the span (thus reducing the AR) is similar to an exponential function. Figure **38** shows that tendency.
- For a constant span, the increase in the flutter speed when increasing the root chord (thus reducing the AR too) is similar to a straight function. Figure **39** shows that tendency.

For higher root chord values the exponential behavior increases little by little (see Figure **38**) while, in the other case, the same happens with the linear tendency when reducing the span (see Figure **38**).

Again, the highest and the lowest flutter velocity condition are compared to the original wing dimensions. Table **10** shows the results.

First of all, according to the results in this subsection, it is clear that the AR affects considerably the flutter instability. Being the values chosen for the span and chord realistic, the changes in the speed are very noticeable, much more than in the previous study.

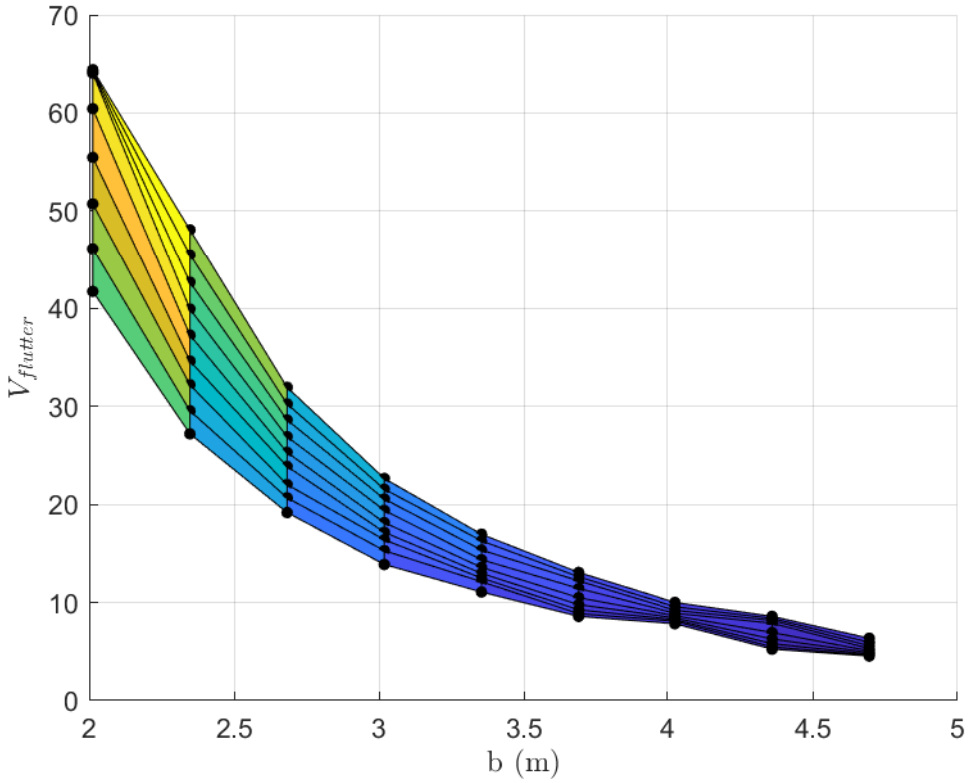

Figure 38 Flutter speed vs b for constant c_r values (side view of the 3D surface plot).

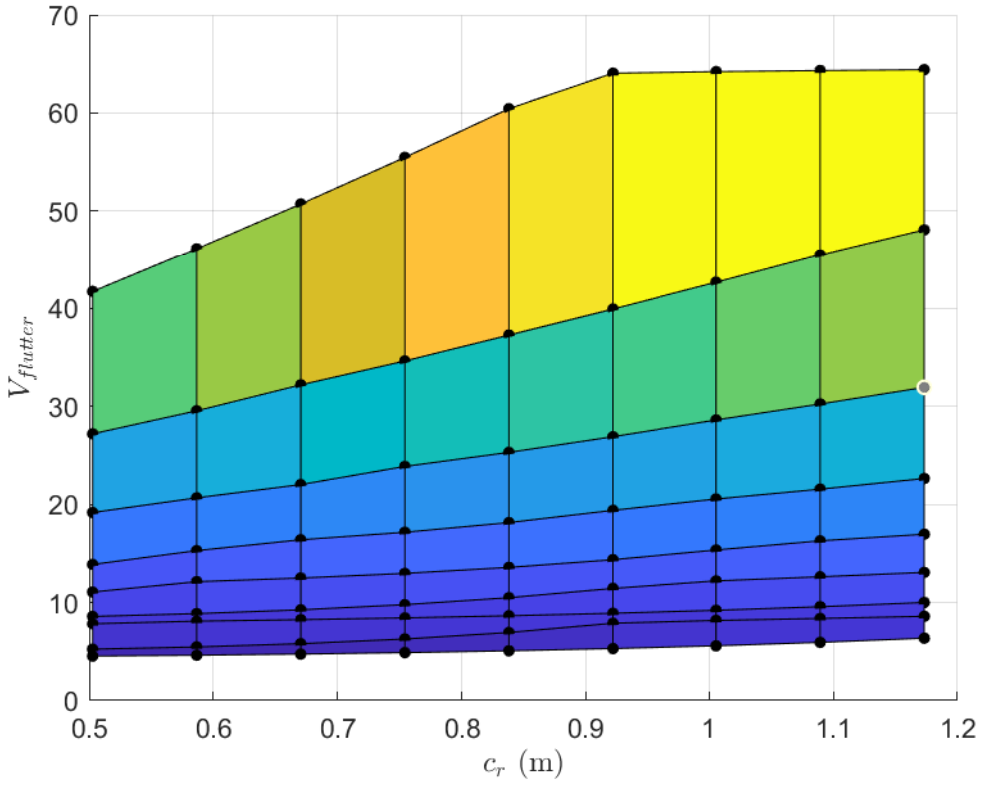

Figure 39 Flutter speed vs c_r for constant b values (side view of the 3D surface plot).

Moreover, more than the AR, it can be said that what affects the instability so much is the wing's planform. A longer but narrower wing would suffer from flutter much sooner than a shorter but wider one.

This last statement is directly related to what was said at the beginning, that one AR can be achieved by two combinations of the span and chord dimensions, one being longer and narrower while the other being shorter but wider. The flutter condition would be most critical for the longer wing, demonstrating what matters most is the plan form of the wing.

5.3.3 Point mass

The last of the three parametric cases considered consists of adding a point mass on some quadrilateral elements of the wing mesh. Two values of point mass will be tested, corresponding to 25% and 50% of the wing mass computed in subsection 3.1.4.

The shape of the wing is the same as the original one so that nor the TR neither the SW nor the AR modifications affect the point mass influence over flutter.

25% M_{wing} point mass

The first point mass corresponds to the 25% of the original wing, being

$$m_{p_{25}} = 15.9037\,kg \tag{5.2}$$

where the subscript p stands for *point*.

This point mass is applied in two different ways:

- On every element of the discretized mesh, so it is only necessary to divide its value by four, the number of nodes that make up the element. For example, if applied on the first element, the nodes [1 2 13 12] will receive $3.9759\,kg$ each.
- Every four elements of the discretized mesh. The value will be divided also by four but, for example for the first element, the nodes affected will be [1 3 25 26], being these the corner nodes of the region covered by the first two elements in both the x and y directions.

On the one hand, Figures **40**, **41** and **42** represent the case in which all the elements withstand the point mass while Figure **43** represents the other case.

One of the reasons to study these two situations was to identify whether the behavior was the same, with this kind of jump in the flutter velocity in the elements closer to the LE and the tip chord.

Notice that, to compute the x and y-axis, which give the percentage of the chord and the percentage of the span where the point mass is applied, a mean position should be found. The mass contributes to four nodes, which make up a rectangular element, so the easiest way to consider it is to compute the middle point in both directions and calculate the percentages there.

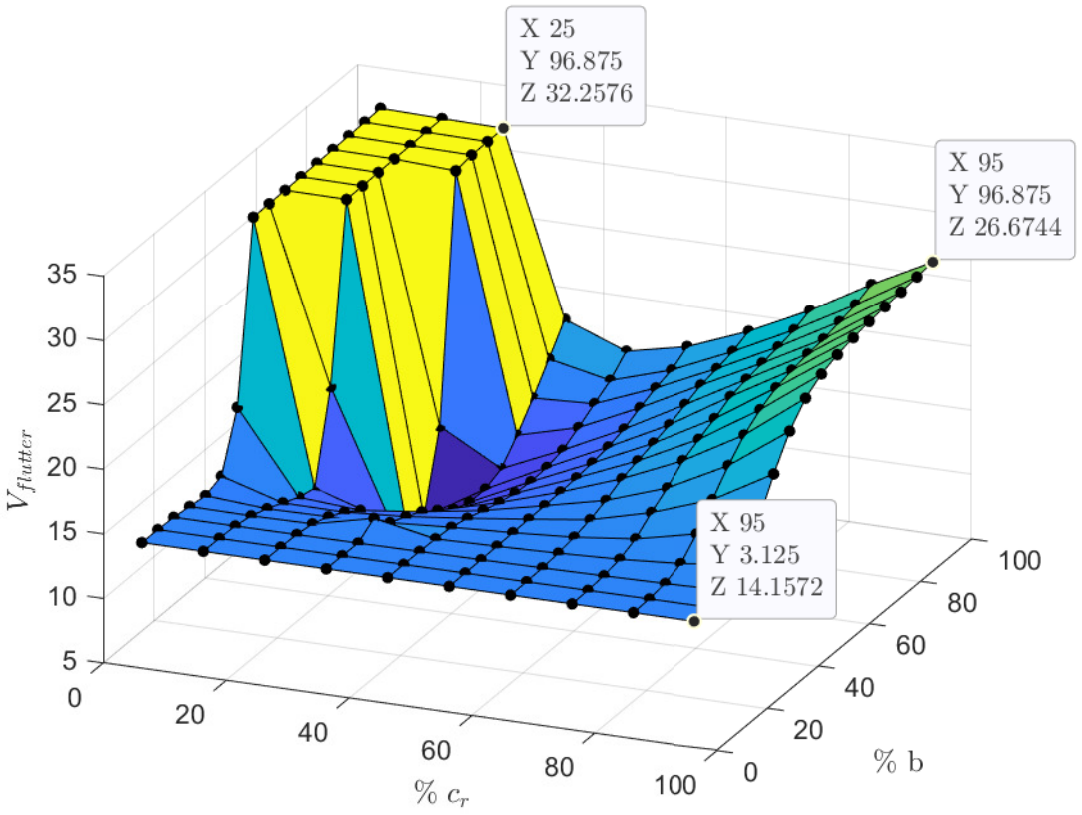

Figure 40 Flutter velocity conditions for a 25% M_{wing} point mass in each of the wing elements.

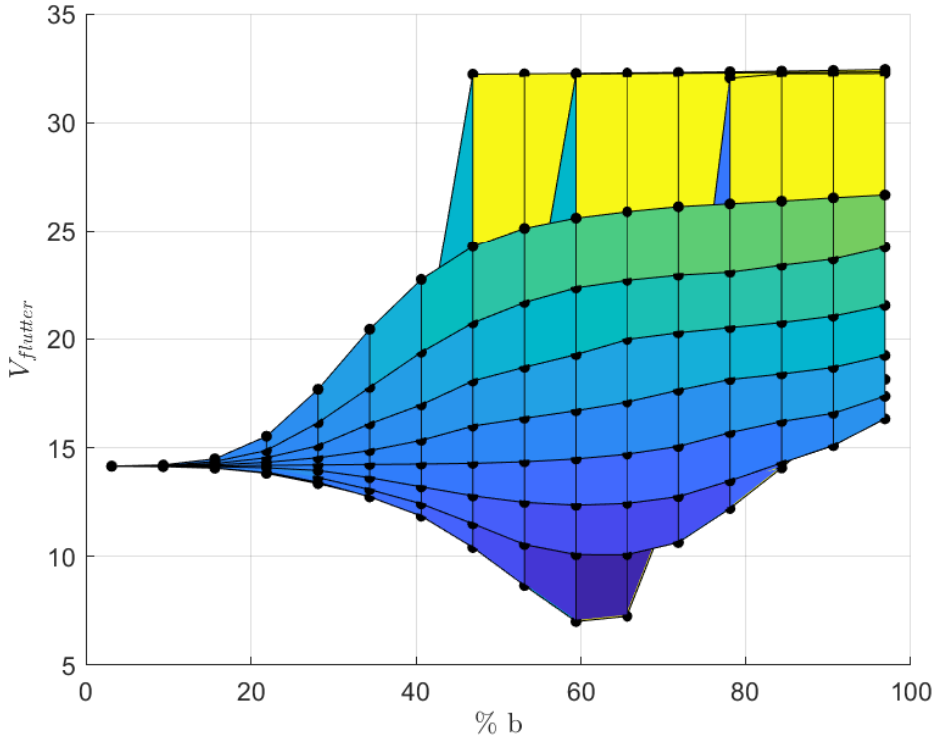

Figure 41 Flutter speed vs %b location of the 25%M_{wing} point mass for constant %c_r values (side view of the surface 3D plot).

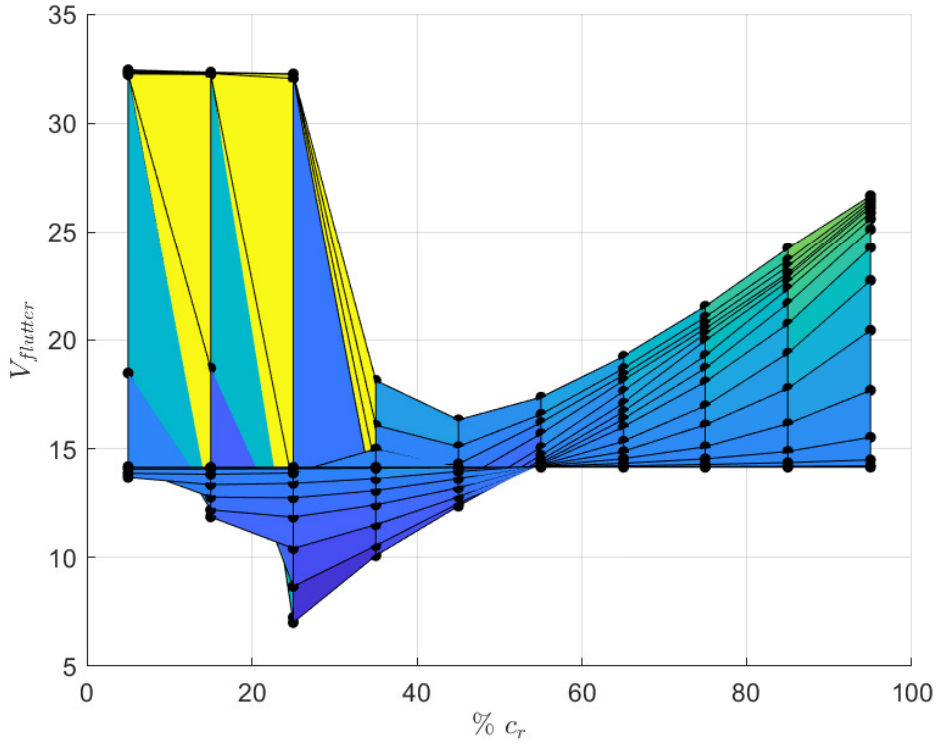

Figure 42 Flutter speed vs $\%c_r$ location of the $25\%M_{wing}$ point mass for constant $\%b$ values (side view of the surface 3D plot).

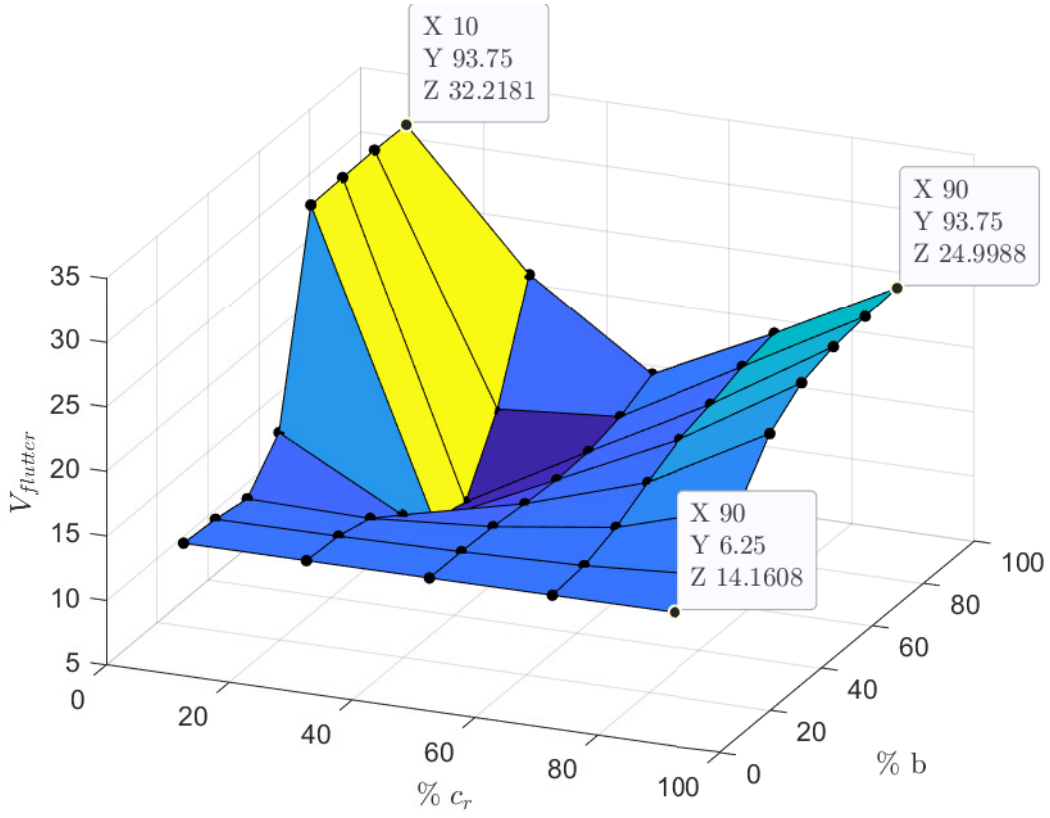

Figure 43 Flutter velocity conditions for a $25\%\, M_{wing}$ point mass every 4 elements of the discretized mesh.

The span percentage for the case in which all the elements are considered goes from 3.125% to 96.875% (16 elements) and the chord percentage goes from 5% to 95% (10 elements).

On the other hand, for the case in which a quarter of the elements are considered, the span points go from 6.25% to 93.75% (8 points) and the chord ones go from 10% to 90% (5 points).

The appearance of the discontinuity observed in the 3D surface plot is due to a change in the flutter condition eigenmode. All the flutter speeds that are included in the flat surface of the elements closer to the tip chord and LE suffer the instability in mode 1, which is a bending-twist mode. Then, for the other elements the behavior is the following:

- The elements that are in the range between 35% and 55% of the root chord c_r suffer flutter in mode 3, a pure twisting mode.
- The elements that are in the range between 3.125% and 28.125% of the span b also suffer flutter in mode 3.
- The elements that are in the range between 65% and 95% of the root chord c_r and between 3.125% and 28.125% of the span b suffer flutter in mode 1.

It is seen that mode 1, a bending-twisting mode, is more difficult to induce flutter in the wing because it needs higher velocity to develop the instability.

50% M_{wing} point mass

The methodology is the same as for the previous case. However, the point mass is now

$$m_{p_{50}} = 31.8074\,kg \tag{5.3}$$

The idea is to analyze whether increasing the value of the point mass affects the flutter condition. Figures **44**, **45** and **46** depict the case in which the point mass is applied on all the elements while Figure **47** depicts the case in which the mass is applied every four elements.

As the figures show, the results for both cases are very similar. The tendency is the same, a surface plot that contains a discontinuity that produces a jump in the flutter velocity when the point mass is applied on elements closer to the LE and to the tip chord. Table **11** compares three flutter conditions for the 25% and 50% M_{wing} point mass.

Furthermore, some general comments on the behavior of the 3D plot can be extracted:

- The flutter speeds are very similar in the two cases (25% and 50% wing mass), the difference is less than 2%.
- The discontinuity includes more elements when increasing the point mass, specially in the span direction.
- For a constant % c_r the tendency of the flutter condition is to increase when getting closer to the tip chord (increasing % b).

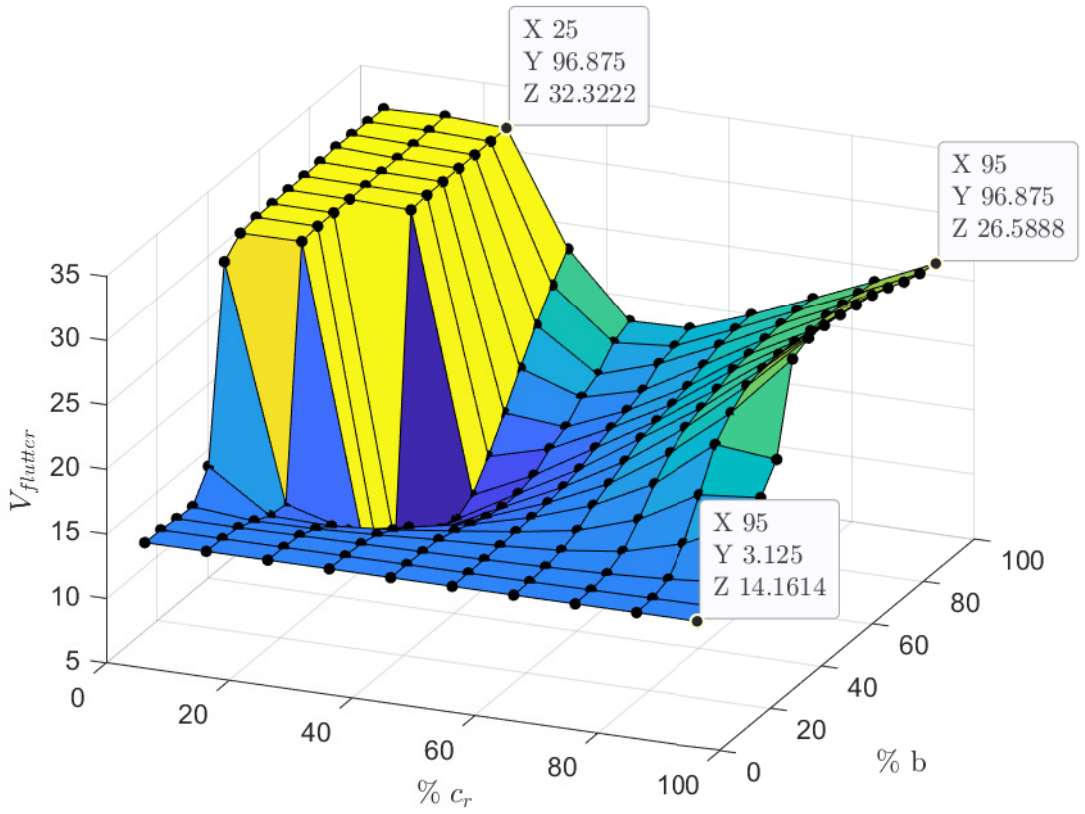

Figure 44 Flutter velocity conditions for a 50% M_{wing} point mass in each of the wing elements.

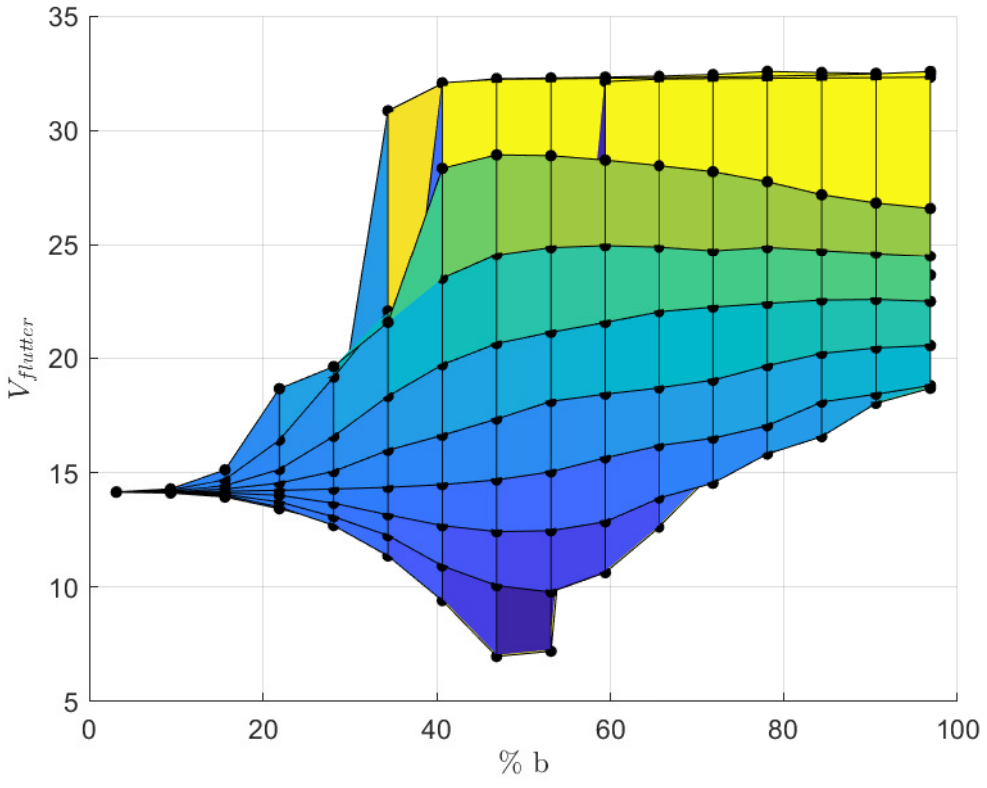

Figure 45 Flutter speed vs %b location of the 50%M_{wing} point mass for constant %c_r values (side view of the surface 3D plot).

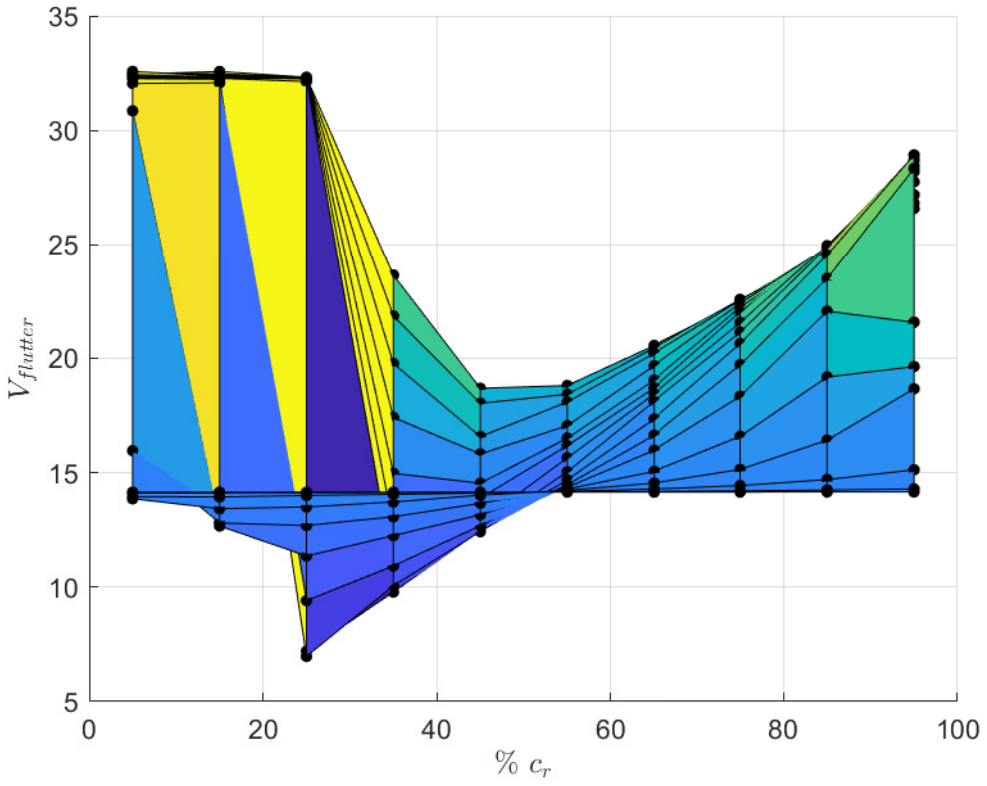

Figure 46 Flutter speed vs $\%c_r$ location of the $50\%M_{wing}$ point mass for constant $\%b$ values (side view of the surface 3D plot).

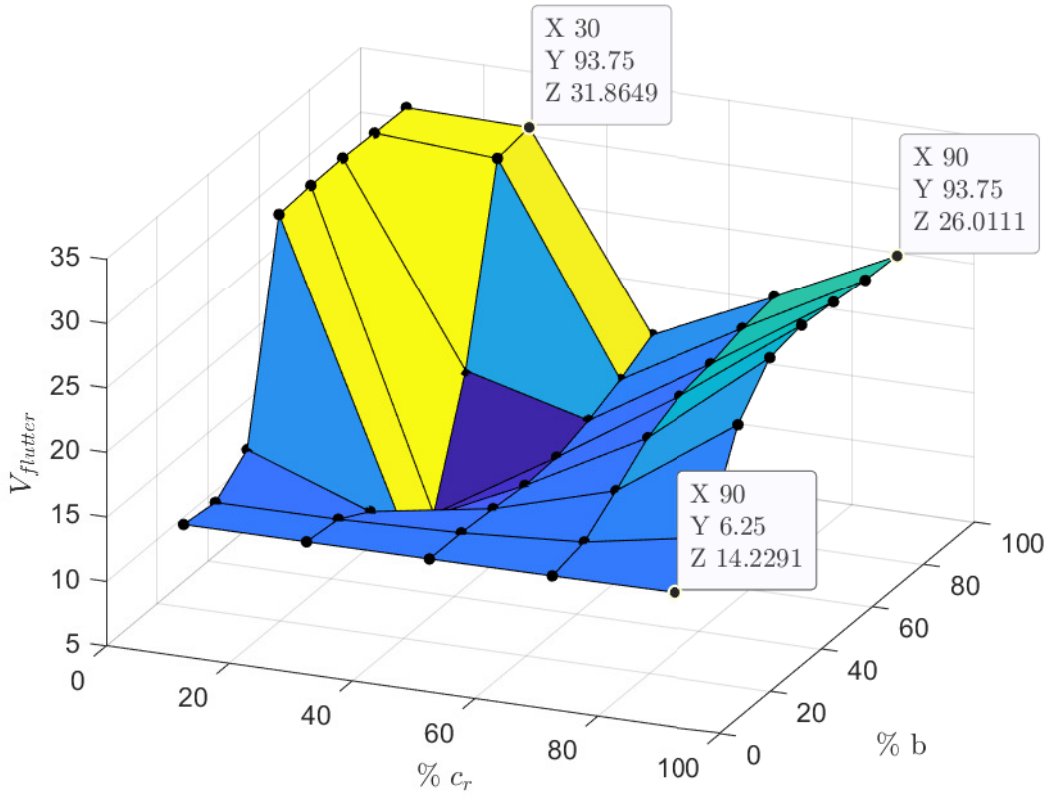

Figure 47 Flutter velocity conditions for a $50\%\, M_{wing}$ point mass every 4 elements of the discretized mesh.

Table 11 Comparison between the original flutter velocity and the TE-root chord, TE-tip chord and close to LE-tip point mass elements.

Point Mass (kg)	Element Location (% b - % c_r)	$V_{flutter}$ (m/s)	% $V_{flutter}$ Original
15.9037 ($25M_{wing}$)	3.125 - 95	14.1572	0.1
	96.875 - 95	26.2744	85.4
	96.875 - 25	32.2576	127.6
0	**0 - 0**	**14.1701**	**100**
31.8174 ($50\%M_{wing}$)	3.125 - 95	14.1614	0.1
	96.875 - 95	26.5888	87.6
	96.875 - 25	32.3222	128.1

- For constant % b the tendency of the flutter condition, when reducing the % c_r, is to start decreasing, get to a minimum and start increasing afterwards.

Finally, taking a look at the 3D surface plots of the second case, where the point mass was applied every four elements of the wing's mesh discretization, one can tell that the behavior is the same as for the first case, where all the elements were considered. Apart from that, the flutter speeds do not differ more than 5% with respect to the first case.

5.3.4 Boeing 737-800 wing planform

The last part of the parametric study is to adapt the mesh to the most realistic wing shape possible. It is true that the wing has been treated as flat and the mesh is simple compared to a real wing but the TR, the SW and the point mass simulating an engine are good indicators of the flutter unstable condition.

There are plenty of different airplanes flying nowadays but, in this case, the Boeing 737-800 is the vehicle chosen. This decision is taken because inside the Boeing 737 family, which has been producing planes since the late 60s, it is the model that has been produced the most, followed closely by the newest model, the Boeing 737 MAX[1].

First of all, according to [9] the TR and the SW of the B737-800 are:

$$\begin{aligned} TR_{737-800} &= 0.159 \\ SW_{737-800} &= 25^\circ \end{aligned} \tag{5.4}$$

Then, the AR needs to be modified too. For the B737-800, considering all the wing, it is

$$AR_{737-800} = 9.45 \tag{5.5}$$

but one needs to take into account that, when considering half of the wing, this parameter needs to be divided

[1]The Boeing 737 MAX first flew in 2016, so all the planes requested are being manufactured right now, they are not flying yet.

by two because of the following:

$$AR_{full} = \frac{b_{full}^2}{S_{full}} = \frac{b_{full}^2}{\frac{(c_r+c_t)\,b_{full}}{2}} = \frac{2\,b_{full}}{c_r+c_t} \tag{5.6}$$

$$AR_{half} = \frac{2\,b_{half}}{c_r+c_t} = \frac{2\,\frac{b_{full}}{2}}{c_r+c_t} = \frac{b_{full}}{c_r+c_t} = \frac{AR_{full}}{2} \tag{5.7}$$

So, according to the demonstration just done, the AR considering half of the wing is 4.725. If the original dimensions of the span and the root chord give an AR (considering the TR and SW of the B737-800) of

$$AR\,(TR = 0.159, SW = 25°) = \frac{2\,b}{c_r+c_t} = \frac{2\,b}{c_r\,(1+TR)} = 6.907 \tag{5.8}$$

This means the span, the root chord or both need to be changed. The ratio which must not change though, being $AR = 4.725$ and $TR = 0.159$, is:

$$\frac{b}{c_r} = \frac{AR\,(1+TR)}{2} = 2.7381 \tag{5.9}$$

At this point, infinite solutions can be selected. However, what is better is to fix either the span or the root chord and see what happens. The dimensions for both cases would be:

$$\begin{aligned} b &= 3.354\,m \qquad & c_r &= 1.2249\,m \\ b &= 2.2946\,m \qquad & c_r &= 0.838\,m \end{aligned} \tag{5.10}$$

As seen in the parametric 3D surface plots it is clear that to avoid flutter a shorter wing is better. That is why, the selected case is the second one, maintaining the root chord and modifying the span.

Before showing the flutter speed result, the point mass needs to be computed. Both the location and the weight of it should be determined. The process to get these values for the B737-800 is presented below:

- **Engine Mass:** According to [9], the power plant that the aircraft uses is the CFM56-7 and taking a look at Figure **48** it only has one engine per semi-wing. Its weight is $M_{e,737} = 2380\,kg$ [10]. Now, to apply it to the wing in this project, a parametrization of this weight needs to be made. One option is to divide the weight by the total semi-wing weight of the B737-800.

  According to [11], the structural mass of the Boeing 737 plane is $M_{w,737} = 10687\,kg$. Therefore, the engine to semi-wing weight ratio gives

  $$\frac{M_{e,737}}{M_{w,737}} = 0.4454 \tag{5.11}$$

  where the subscripts e and w refer to *engine* and *wing*.

- **Engine Position:** Figure **48** shows the front view of the airplane with some important dimensions. The semi-span is $17.90\,m$, while the farthest point from the engine with respect to the beginning of the

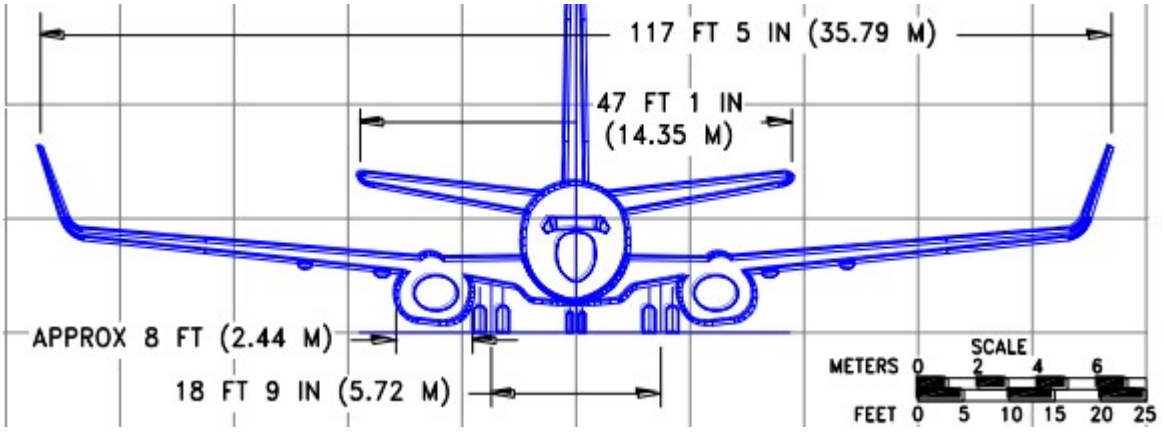

Figure 48 Boeing 737-800 front view and dimensions. (Source: [12])

wing is located at a 5.3 m distance. Another time, making use of a ratio, one gets

$$\frac{b}{d_{e,737}} = 0.2960 \tag{5.12}$$

The last step is to apply the weight and distance ratios to the wing studied in the code. Regarding the weight, the mass of the wing when TR and SW are implemented has not been computed. So to avoid integrating another time, as it is mentioned in subsection 3.1.4, the weight is approximated to the % of the surface with respect to the original one. This way,

$$M_{wing}(TR = 0.159, SW = 25, AR = 4.725) = \frac{S_w}{S_{w,orig}} M_{wing}(TR = 1, SW = 0, AR = 4) = 25.22\,kg \tag{5.13}$$

and using this number the engines mass is 11.2329 kg.

On the other hand, the engine's equivalent point mass would be ideally applied at 29.6% of the wing semi-span. However, it needs to be implemented over nodes and none of the nodes are at this position. Because the point mass is applied at the center of an element, the closest ribs are 5 and 6, being their middle point at 28.125% of the wing semi-span.

Finally, as the engines tend to have the air intake before the LE, the point mass will be applied as close to the LE of the wing as the mesh will let, being the first two horizontal elements (5% c_r beyond the LE).

Summarizing, the point mass will be placed at the element whose nodes are [45 46 57 56] and its middle point at 28.125% of the root chord and 5% of the LE.

Figure **49** and Table **12** show the flutter plot and the flutter speed condition that arise from considering the Boeing 737-800 parameters over the original wing shape.

Table 12 Flutter condition for the equivalent of the Boeing 737-800 wing shape.

V_{flut} (m/s)	Eigenmode	Type of Motion
43.4777	5	Twisting

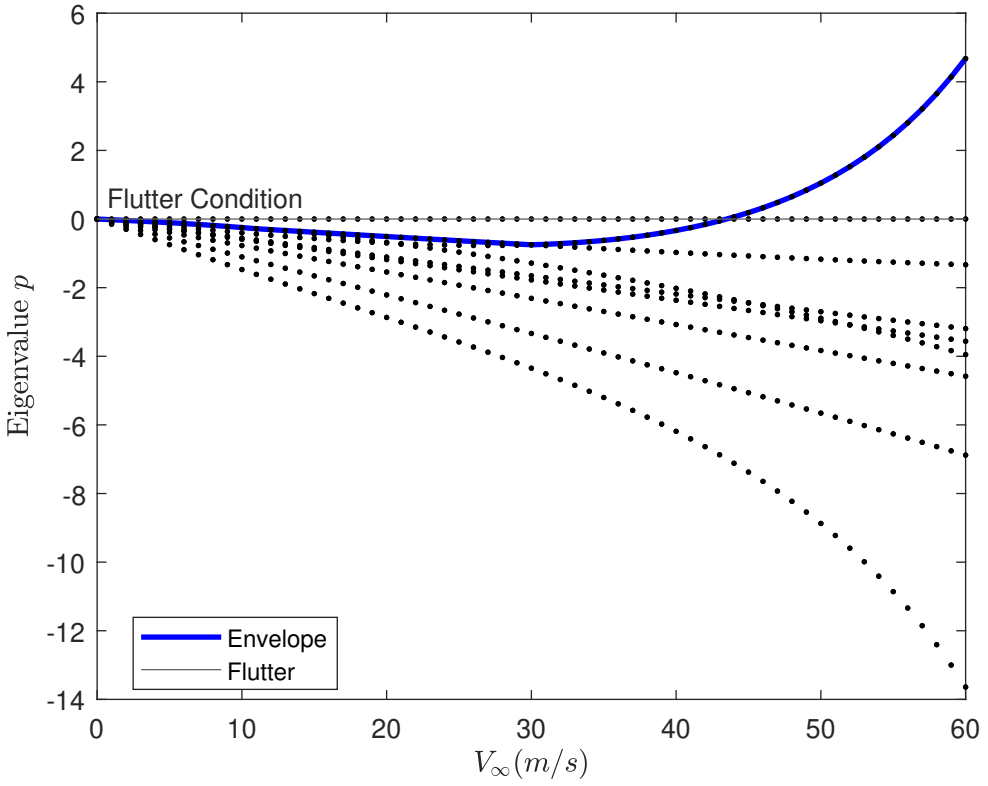

Figure 49 Mode plotting and flutter condition for the Boeing 737-800 wing shape ($TR = 0.159$, $SW = 25°$ and $AR = 4.725$) adding the equivalent to an engine mass in the $\approx 28\%\, b$ - LE element.

Notice that, as for the original wing shape flutter plot, twisting is the type of motion that trigger the instability. Furthermore, the flutter speed is almost three times the original one, being the wing shortening the most important influence.

Chapter 6

Conclusions & Future Work

Finally, when the case is studied and solved, one of the most important parts relies on extracting adequate conclusions and defining a future path for someone who would be interested in extending the work.

Therefore, technical and personal conclusions are presented below, together with a guide for anyone interested in giving continuity to the project.

6.1 Conclusions

6.1.1 Technical conclusions

First of all, it is important to highlight that the study has been a success. The aim of the project was to develop a computational code that gave the flutter condition for a determined wing structure and it has been achieved. Moreover, all items in the scope have been accomplished, for example, the structural and aerodynamic codes have been validated separately before developing the coupled code, ensuring that the results obtained are correct.

Regarding the shape of the wing, the dimensions were picked from a code developed by a NASA researcher so that the validation of the structural and aerodynamic models could be done using its tutorials. The validations have been satisfactory, being the first important issue to keep developing the code. It is true that the dimensions are not those of real aircraft wings, they are somehow scaled in order to simplify the complexity of the mesh.

In terms of the mathematical models implemented there is a noticeable difference between the structural and aerodynamic formulations. The structural model is strong, it is complex and considers the 3D extension for future developments. Although the wing is 2D, the 3D case is already prepared if a more detailed mesh is to be studied. On the other hand, the aerodynamic model is based on vortex elements that solve the potential flow problem. Therefore, the flow is inviscid, steady and incompressible. Unsteady, compressible hypotheses increase considerably the complexity of the solution and are out of the scope of this work.

Then, the P-Method allowed to develop the aeroelasic coupling. It is important that the aerodynamic formulation did not need to be changed using this method. Because of that the solution of the flutter instability is quasi-static and not unsteady at all but extending the steady to unsteady would increase a lot the difficulty of the problem.

Once the code was developed and run the parametric study started. The parameters changed were the taper ratio, the sweep angle, the aspect ratio (by changing the span and chord lengths) and the addition of a point mass in some elements.

For the taper and sweep the expected behaviors have been proved. The sweep angle reduces the incident velocity on the wing surface so the flutter speed increases. The tapper ratio affects directly the influence of the lifting force, the smaller its value, the more influence there will be near the root chord. Therefore, the flutter speed also increases. For both of the parameters flutter appears in a twist mode.

With respect to the aspect ratio, the results show what one would expect initially. By reducing the span length thus reducing the aspect ratio, flutter is less probable to appear, its velocity increases. This is because the stiffness is increased. The same happens when increasing the chord and maintaining the span length, the aspect ratio is decreased and the flutter speed increased. The mode in which flutter appears is also a twist one.

The effect of modifying the aspect ratio is greater than that of modifying the taper ratio and wing sweep, meaning that it affects more the stiffness property.

Finally, adding a point mass in some of the wing discretized elements affects flutter in an unexpected way. When the element is closer to the wing tip chord and to the leading edge the instability appears in a bending-twist mode. The flutter speed is more than two times the one obtained for the original wing shape without changing the parameters. However, when the elements are closer to the root chord the mode that activates flutter is pure twisting and between the leading and trailing edge spars the same.

This behavior has to do with the distance between the center of gravity and the elastic center. It affects flutter considerably and in this case the mass added is not negligible, it corresponds to a noticeable percentage of the wing's mass.

A last results was sought, one trying to imitate a scaled real-aircraft wing. That implies a modification in the four parameters considered at the same time. Being the taper small, the sweep high, the span length reduced and the point mass simulating the engine close to the leading edge, the combination gives a high flutter speed, which is good for the aircraft because it would delay the instability appearance.

6.1.2 Personal conclusions

This project has been one of the most challenging experiences I have ever faced in my entire academic life. Facing a completely new subject for me, which is even beyond the majority of the knowledge acquired during the degree, has made me realize how much I am capable of doing right now. It is true that without the effort of my tutors it would have not been possible. They have taught me a lot of things I did not know and

that were necessary to achieve the results, I am very grateful for their work. I have learnt so much and only because of that I am very proud.

My first objective when beginning the project was doing something related to the aerodynamics and structural fields. Then, it had to be something that taught me new things, it was a priority for me to learn, and to learn a lot. Looking back, I believe it has opened up an amazing world for me, the computational field fascinates me and I know that one way or another I will work on something related to it in the future.

On the other hand, it has also been a challenge to combine the internship in a company with the development of the project. In my opinion, it has helped me a lot to organize all the activities better. Carrying out works like that teach you discipline, teach you to sacrifice time doing other things you would prefer, but if you are proud of what you have achieved at the end then the job is done.

6.2 Future Work

The code developed in this work is far from being finished, there is always something one can improve. For example, the aerodynamic model is simple because it has been implemented using the potential flow hypothesis. This would be the one of the possible developments, to introduce a more realistic model including compressible flow and wind gusts, transforming the problem into transient regime.

Then, different flight altitudes can be studied, a flying altitude range to decide at which it is best for the aircraft to avoid the flutter instability. Apart from that, camber can be added because the wing has been created as a flat plate and considering an aerodynamic profile section would be much more accurate. With these options, the aerodynamics and the structural models would be both complex enough to simulate a real semi-wing.

Although, as mentioned previously, the structural model is more complex and accurate than the aerodynamics one, improvements can be made. The first one has to do with adding camber to the flat plate. This would involve an additional difficulty when computing the stiffness and mass matrices. Moreover, 3D structural elements could be implemented, being the mesh highly complex to be created manually. An external program such as ANSYS or GID would be required.

Furthermore, the spars and ribs could be considered with I cross sections and holes to lighten the total weight of the wing. New materials can be defined so not to consider the wing with uniform properties. This would affect the flutter condition for sure, because the stiffness and center of gravity of the wing are two key issues regarding the instability.

On the other hand, regarding the coupling systems it would be interesting if the P-Method implemented is compared to the P-K Method thus two different solutions for the flutter condition would be given. In relation to the latter, the solution obtained by running a CFD analysis of the flow around the wing would be also intriguing.

Referring to the results analyzed, it would be challenging to include, for each combination of parameters, the first flutter speeds for both bending and twisting motion. Not only the first flutter speed is important to

know, which of course is the most critical one, but also the ones that correspond to other types of motion.

Finally, real wing dimensions con be also analyzed. To know the flutter conditions of real aircraft wings could be intriguing. Studying then their cruise velocity, for example, would help make rough predictions of the security margins established in the aeronautics field.

It is clear that this study has provided a first approach to the appearance of the flutter instability in an aircraft wing. However, there are lots of ways to improve or extend the code so that different solutions are obtained. Different paths can be taken towards computing more results or refining the theory models, for example. It has the potential to grow and become a tool in the academic environment, being useful to students and/or professors who may cross paths with the flutter instability.

References

1. KATZ, Joseph; PLOTKIN, Allen. *Low-speed aerodynamics*. Cambridge university press, 2001.
2. WRIGHT, Jan Robert; COOPER, Jonathan Edward. *Introduction to aircraft aeroelasticity and loads*. John Wiley & Sons, 2008.
3. HODGES, Dewey H; PIERCE, G Alvin. *Introduction to structural dynamics and aeroelasticity*. Cambridge University Press, 2011.
4. CAPPONI, Castillo. A Finite Element Approach for Aeroelastic Instability Prediction of Wind Turbines. 2010.
5. SUH, Peter; MAVRIS, Dimitri. Modal filtering for control of flexible aircraft. In: *54th AIAA/ASME/ASCE/AHS/ASC Structures, Structural Dynamics, and Materials Conference*. 2013, p. 1741.
6. INTERNATIONAL, ASM. *Metals Handbook Vol. 2: Properties and Selection: Nonferrous Alloys and Special-Purpose Materials*. ASM, 1990.
7. ROCA, David. *Computational Engineering: FEM Beam Elements*. Universitat Politècnica de Catalunya, February 2022.
8. ROCA, David. *Computational Engineering: FEM Plate and Shell Elements*. Universitat Politècnica de Catalunya, February 2022.
9. BRADY, Chris. *The 737 Information Site*. 1999. Available also from: `http://www.b737.org.uk/techspecsdetailed.htm`. Accessed: 10/06/2022.
10. EASA. Type Certificate Data Sheet for Boeing 737. *RED*. 2016, vol. 3, p. 102.
11. ARDEMA, Mark D; CHAMBERS, Mark C; PATRON, Anthony P; HAHN, Andrew S; MIURA, Hirokazu; MOORE, Mark D, et al. Analytical fuselage and wing weight estimation of transport aircraft. 1996.
12. BOEING. *737 Airplane Characteristics for Airport Planning*. Boeing Commercial Airplanes, October 2021.